NOTE TO USERS

Characterization of Material Surface by Using Fiber Bragg Grating

Jun Chen

A Thesis

in

The Department

of

Electrical and Computer Engineering

Presented in Partial Fulfillment of the Requirements
for the Degree of Master of Applied Science
(Electrical and Computer Engineering) at
Concordia University
Montreal, Quebec, Canada

March 2005

Canada

ABSTRACT

Characterization of Material Surface by Using Fiber Bragg Grating

Jun Chen

Fiber optic sensors based on Fiber Bragg Grating (FBG) technology are found to be a promising technique for measuring parameters like strain, temperature, pressure, vibration, acceleration etc. However, few investigations in displacement measurement using FBG were reported. Most works reported in the literature are related to the displacement measurement in the range of mm. In this thesis, a fine displacement measurement using Fiber Bragg Grating (FBG) is proposed. A FBG sensor is regarded as a promising candidate to be applied to surface measurement instrumentations due to its dual sensing abilities for force and for displacement, small sensing part in size, simple uniaxial measurement configuration, linear responsive behavior and simple measurand interpretation. Because the optical fiber technology is used, FBG sensors applied in material surface characterization may offer a series of advantages over conventional electrical sensors such as the immunity from electromagnetic interference. In the field of material surface characterization, because FBG can sense both the displacement and the force against the substrate, it has the capability to be used not only in surface topography measurement but also in the indentation measurement to investigate the dynamical mechanical properties of the substrate material.

To the best of our knowledge, no work using FBG appeared in the literature on the fine measurement in the scale of micro or less.

The purpose of this thesis is to establish a new methodology to characterize

material surface by using the Bragg grating fiber technology into micro and sub-micro scales. Three measurands are proposed in the thesis, indentation measurement using one-FBG, indentation measurement using two-FBG and step height measurement. Theories for the new methods are derived and the experiments are implemented. To achieve fine scale measurement, the requirement of large measurement sensitivity is discussed. Monitoring and controlling the force against the substrate is highlighted in the thesis.

ACKNOWLEDGEMENT

TABLE OF CONTENTS

TABLE OF CONTENTS (continued)

TABLE OF CONTENTS (continued)

TABLE OF CONTENTS (continued)

LIST OF FIGURES

LIST OF FIGURES(continued)

LIST OF FIGURES (continued)

LIST OF TABLES

NOTATION AND ABBREVIATIONS

A	*Area. In microhardness measurement, A is the impression area. For fiber, A is the cross section area.*
A_p	The projected contact area at that load
E	The elastic modulus or young's modulus
E_{IT}	The indentation modulus calculated from the slope of the tangent of the unloading curve
E_i	The elastic modulus of the indenter
E_r	The reduced modulus
F	The applied force against the fiber
FBG	Fiber Bragg grating, a sensing element in possession of a periodic modulation of the refractive index in the core of an optical fiber
FBG fiber	A piece of fiber with a FBG in it. The length of FBG fiber $\geq$ the length of a FBG
F_m	The force against M grating fiber
F_{max}	The maximum load of an indentation process
F_s	The force against S grating fiber
F_{sub}	The force against sample.
H	Hardness
h_{dep}	The depth of the probe into the sample or deformation of the material surface
h_{dis}	The displacement of sample approaching to the probe
H_{IT}	Indentation hardness

Notation and Abbreviations(continued)

ISO   The International Organization for Standardization

K_ε A coefficient in the unit of nm/ $\mu\varepsilon$

K_T A coefficient in the unit of nm/°C

K_t A coefficient in the unit of 1/°C

l The length of the fiber

Δl Elongation, the change of the fiber length.

l_0 The length of fiber unloaded

l_1 The length of the FBG fiber with respect to the bottom end of fiber at height 1

l_2 The length of the FBG fiber with respect to the bottom end of fiber at height 2

l_f The length of FBG fiber that is only hung by a certain load, no sample supports

$l_{m,0}$ The length of unloaded M grating fiber

$l_{m,max}$ The length of M grating fiber only loaded by the load

$l_{s,0}$ The length of unloaded S grating fiber

$l_{s,max}$ The length of S grating fiber only loaded by the load.

l_{sur} The elongation of S grating fiber when the load and probe reach the surface of the sample

M grating   The grating used to monitor and control the force

N   Newton, the force unit.

n_{eff} The effective refractive index of the fiber core

nm   Nanometer

OSA   Optical spectrum analyzer

p_e The effective photoelastic constant $p_e = \dfrac{n_{eff}^2}{2}[p_{12} - \upsilon(p_{11} + p_{12})]$ [48]

Notation and Abbreviations(continued)

p_{ij} The fiber Pockel's coefficients

S grating   The grating used to sense the displacement

W The weight of the load

Λ The grating period

δ The offset

ε $\varepsilon = \Delta l / l$, the longitudinal deformation of the fiber normalized by the length of fiber, in the unit of $\mu\varepsilon$

λ_B Bragg wavelength, or the central wavelength of the reflected narrow band light

$\Delta\lambda_B$ The shift in Bragg wavelength in the unit of nm

λ_0 The reflected wavelengths of FBG fiber without strain

λ_1 The reflected wavelength of the FBG fiber with respect to the bottom end of fiber at height 1

λ_2 The reflected wavelength of the FBG fiber with respect to the bottom end of fiber at height 2

λ_f Tthe reflected wavelengths of FBG fiber that is only hung by a certain load, no sample supports.

$\lambda_{m,\,min}$ The shortest reflected wavelength from M grating, which is related to no strain, no fiber elongation and no reflection shift of $\Delta\lambda_{m,\,min} = 0$

$\lambda_{m,\,0}$ $\lambda_{m,\,min}$

$\lambda_{m,\,max}$ The longest reflected wavelength from M grating, related to maximum strain on M grating, fully elongated by the load and had the maximum reflection shift of $\Delta\lambda_{m,max}$

$\lambda_{m,s}$ The reflected wavelength of M grating when the probe just reach the sample.

$\lambda_{s,\,min}$ The shortest reflected wavelength from S grating, which is related to no strain, no fiber elongation and no reflection shift of $\Delta\lambda_{s,\,min} = 0$

$\lambda_{s,\,0}$ $\lambda_{s,\,min}$

Notation and Abbreviations(continued)

$\lambda_{s,\,max}$ The longest reflected wavelength from S grating with the maximum reflection shift of $\Delta\lambda_{s,\,max}$

$\lambda_{s,sur}$ The reflected wavelength from S grating when the load and probe reach the surface of the sample

$\frac{d\lambda}{dl}$ The measurement sensitivity because it describes how sensitive the sensor is when it responses to a unit displacement

$\frac{d\lambda}{dF}$ The force sensitivity

$\mu\,\varepsilon$ Microstrain

ν Tthe Poisson's ratio of fiber

ν_i The Poisson's ratio of the indenter

ν_s The Poisson's ratio of the tested sample

CHAPTER I

OVERVIEW AND BACKGROUND

In modern industry, surface-treated and surface-coated material plays an important role. Characterization of surface properties for quality control of the coated and modified layers requires varied measuring techniques[1,2]. The interesting size has been gone into the micro scale, sub-micro scale or even into the nano scale. Marvelous instrumentations have been developed and are still being developed to meet needs for the small region investigation. Among them there is a class of instrumentation using hard probe, emerged to detect the surface properties. This instrumentation class arms at two major goals: surface topography measurement and the indentation measurement[3,4,5,6,7]. The former features the vertical changes of the material surface, which can measure the film thickness, wear scar, step height, etched depth and surface roughness. The latter offer the information about the material mechanical properties, such as the microhardness and elastic modulus. Both instruments use a diamond tip or other stiff tips as the hard probe to contact the surface of the tested material while measuring. In the topography measurement, the probe, always called stylus, makes contact with the material surface but applies the force against the surface as less as possible, whereas in the indentation measurement the probe, always called indenter, has to indent into the surface and obtains the material information by changing the applied force against the surface of the material. Controlling the applied force and sensing the displacement of the probe is the most importance in both instrumentations. This thesis introduces the fiber Bragg grating (FBG) to sense these two parameters. In this thesis, we present a method to use FBG to measure the indentation measurement on a

1

surface as well as the topography measurement. In this chapter, the background of the optical fiber, FBG, displacement measurement using FBG and the surface measurement techniques using a hard probe are briefly presented. The scope and thesis presentation is brought at the end of this chapter.

1.1 Background of the Optical Fiber and Bragg Grating

1.1.1 The Fiber Optic Evolution and Transmission Windows

The fiber optic technology has grown rapidly since its successful inception in communication in 1970's[8,9]. It has revolutionized the telecommunication network due to its outstanding advantages. According to Charles K. Kao, one of the pioneers of glass fibers for optical communications, "the low-transmission loss and the large bandwidth capability of the fiber systems allow signals to be transmitted for establishing communications contacts over large distances with few or no provisions of intermediate amplification[8]."

The optical fiber application evolves based on the attenuation characteristic of the optical fiber [9,10], shown as in Fig.1.1. The first generation operated through a low transmission window of early silica fiber at the range of 800-900 nm, which is referred to as the first window used for the optical telecommunication. By reducing hydroxyl ions and metallic impurities in the fiber, it was able to be fabricated with very low loss in the 1100 – 1600 nm region referred as the long wavelength region. In the long wavelength region although in 1998 the optical fiber eliminated the 1400 nm attenuation peak was appeared, there are still two optical windows in recently common use, which are the second window around 1310 nm and the third around 1550 nm because between 1310 nm and 1550 nm there is a water molecule attenuation peak around 1400 nm.

2

Communication has shifted from transmission wavelength of 800nm to 1310 nm
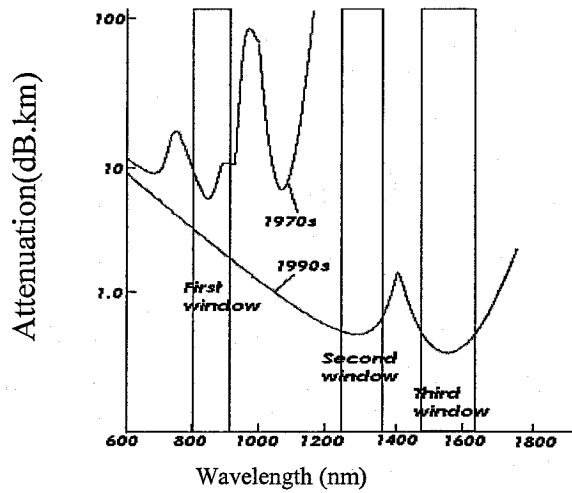
Fig1.1 Optical fiber attenuation as a function of wavelength[9,10]. Early fiber was used in the 800 to 900 nm range. Lower attenuation was achieved in the longer wavelength windows 1310nm and 1550nm.

and then to 1550 nm resulted from developments of relative optical sources, photodetectors and other devices. The optical fiber technology used in communication is now matured and achieved advantages that others is not able to reach. Take the bit rates as a example. In 1970s, bit rates ranged from 45 to 140Mb/s within 10 km. In 1980s by using 800 nm technology, bit rates ranged from 10 to 100 Mb/s over distance of tens of kilometres by using 800 nm technology. Then, 1550 nm system can carry traffic at around 2.5 Gb/s over 90 km. by 1996, advances in high-quality lasers and receivers allowed single wavelength transmission rates of 10 Gb/s in 1550 nm system[9].

In this work, among the three matured windows, the longest transmission wavelength 1550 nm is used because it can obtain the highest sensing sensitivity compared to 800 nm and 1310 nm systems.

1.1.2 Properties of the Optical Fiber

Material used for the optical fiber is silica. The optical fiber is configured as a dielectrical waveguide that operates at optical wavelength. An optical fiber in a cylindrical arrangement comprises two parts with slightly different refraction indexes such as the difference as 0.1%. The center is called *Core*, which is surrounded by a layer called *Cladding*. A practical optical fiber contains additional coatings and jacketing covering the cladding for mechanical strength and protection, not for optical purpose.

This structure of optical fiber confines the light within the core and guides the light to propagate in the direction parallel to fiber's axis.

The ratio of the speed of light in a vacuum to that in the mater is the index of refraction n of the material:

$$n = \frac{c}{v}$$

(1.1)

where $c = 3 \times 10^8$ m/s, a light speed in a vacuum space, v is the light speed in the mater. The difference of the speed of light in two materials with different refractive indices changes the direction of light traveling at the interface between two materials. If n_1 and n_2 are the refractive indices of two materials, at the interface it follows Snell's law

$$n_1 \sin\phi_1 = n_2 \sin\phi_2$$

(1.2)

where the angle ϕ_1 and ϕ_2 are the angles between the incident and the refracted beams respectively with respect to the normal to the surface. If $n_1 > n_2$, then $\phi_1 < \phi_2$. If ϕ_1 is increased, ϕ_2 will also increases. When ϕ_2 reaches 90 °, ϕ_1 becomes the so called critical angle ϕ_c.

$$\phi_c = \sin^{-1}\left(\frac{n_2}{n_1}\right)_{\phi_c}$$

(1.3)

4

When ϕ_1 is greater than the critical angle, the total internal reflection is happened; the light is totally reflected back and does not pass through the interface to escape out of the fiber. Total internal reflection is the mechanism of light propagating along a fiber by using the cladding with n_1 to reflect the light back to the core with $n_2 (n_1 > n_2)$.

1.2 Grating Sensor

1.2.1 FBG Description and Function

The fiber Bragg grating (FBG), as a sensing element, is a small portion in
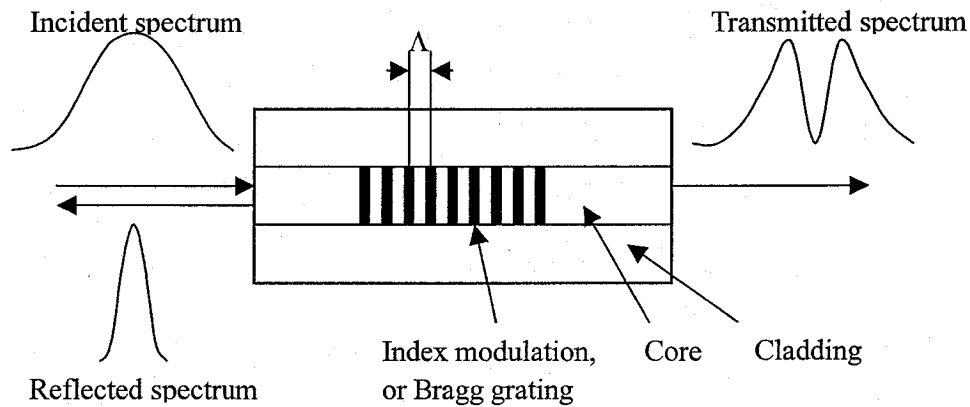
Fig.1.2. FBG in the fiber and its function

possession of a periodic modulation of the refractive index in the core of an optical fiber. The refractive index modulates in the signal propagation direction along the core of the fiber. The typical length of the modified section in the fiber ranges between 6mm and 15mm. FBG is photo-inscribed with UV radiation and specially patterned masks. If a broadband of light launches into the fiber with a FBG as depicted in Fig1.2, the FBG as a selective filter allows all wavelength of light pass forward but a narrow band of light is reflected back, or FBG divides the incident spectrum into the reflected spectrum and the transmitted spectrum. The center of this reflected band from FBG is determined by the

5

periodically modulated arrangement and the modified index. This characteristic center of the reflected band can be detected and measured by instrumentation from the reflected spectrum and from the transmitted spectrum. When the fiber is stretched or compressed along its axis, the FBG section in the fiber is also stretched or compressed and changes its periodicity of the geometrical structure and the value of the refractive index. As a result, the center of the reflected wavelength shifts. Thus, the shift of the reflected wavelength can be used to monitor the strain in the fiber induced by the fiber's stretch and compression. The reflected wavelength and its shift can be detected by using the instrument of optical spectrum analyzer (OSA).

The first report of photosensitivity in optical fiber was attribute to Hill in 1978[11,12]. However, the first practical grating technique was regarded to be UV grating fabrication in 1989[13]. Recently, the rapid progress has been made in both FBG sensor system developments and applications [12,14,15,16,17,18,19].

1.2.2 FBG Fabrication

Currently, there are two major methods for fabricating Fiber Bragg Grating: holographic method[13] and Hill's phase mask method in 1993[20]. In 1989, G. Meltz[13] used holographic interference setup to write FBG, and the grating was written from the side of fiber. The advantage of the Holographic method: it is easy to adjust the angle between two beams to create different periods, therefore, to fabricate FBG with difference wavelengths. The disadvantage of this method is that a more stable setup is needed and a good coherence light source is also requested in the meantime. In 1993, Hill et al gave another easy method to fabricate FBG by phase mask. Phase mask is a piece of diffractive grating with depth modulation on fused silica. The UV beam incident on phase mask and

6

carry a interference pattern to write the FBG on the fiber. The advantage of Phase Mask method: it is simple with great repeatability as well as the disadvantage of Phase Mask: each mask can only generate one wavelength of FBG.

1.2.3 Role of Grating Sensor

When talking about optical fiber sensor, an invited paper should be mentioned, "Review of the present status of optical fiber sensors" written by Byoungho Lee[21]. Optical fiber sensors are reviewed in the paper. Byoungho Lee reported that the most highly discussed measurands are strain and temperature, and fiber grating sensors are clearly the most widely studied topic according to his statistics on the distribution of papers presented at the 15th Optical Fiber Sensors Conference (OFS- 15: IEEE catalog number 02EX533), a major conference in the field of optical fiber sensors, held in Portland, Oregon, USA in May 2002. Distribution of OFS-15 papers according to technologies showed fiber grating was involved in 44.2%, interferometers 11.1%, scattering/reflection 10%, faraday rotation 6.9%, fluorescence/ luminescence/ blackbody 6.6%, FOG 4.4%, low- coherent interferometer 3.5% and others 13.3%. Fiber grating sensor technology is the most popular topic in optical fiber sensors.

1.2.4 Advantages of FBG Fiber Sensor

One of the characteristics of an FBG is that the wavelength of its reflected beam will be shifted if any strain applied on it. This property is used to fabricate strain sensors[22]. The advantages of FBG sensors over conventional electric sensors include [9,22]:

- featured with small size and lightweight;

- susceptive to multiple ambient variances (strain, pressure , temperature,

humidity, vibration and chemicals...);

- immune to electromagnetic interference (available strong electromagnetic field

  and low noise);

- easily multiplexed and largely scaled distributed(many sensor and receiver

  though a whole fiber);

- · mostly linear sensing mechanism(simply analysis) ;

- tolerant of power fluctuation(use of wavelength shift information) ;

- environmentally more stable and durable (free from rust).

1.3 Displacement Sensor Using FBG

There are very few reports available in literature related to displacement sensor
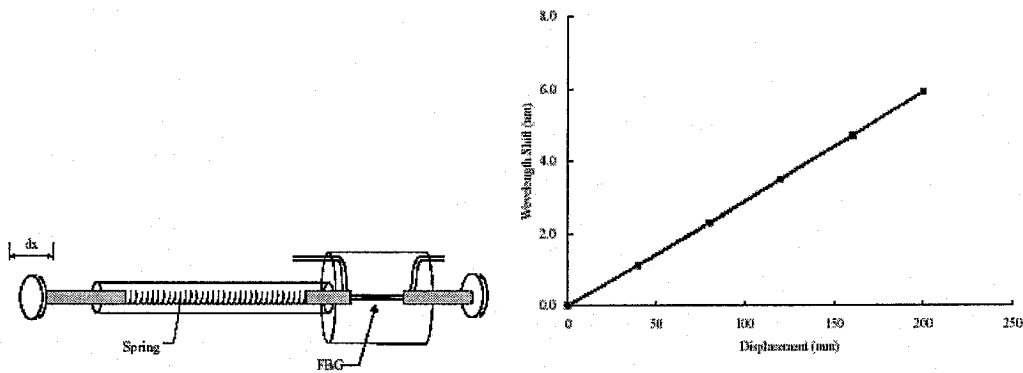
Fig. 1. 3 A diagram of FBG-based sensor for large displacement measurement[23], and the
relation between the displacement and the wavelength shift

using fiber Bragg grating. The reason may be that the absolute displacement directly with

respect to the elongation of FBG is limited. Researchers tried some methods to measure the

displacement much longer than the elongation of FBG.

8

One example is that the FBG element is bonded onto a metal bar that is connected

to a soft spring[23] shown in Fig.1.3. Because the bar and the spring are connected in a

series, more detected displacement is shared by the soft spring and less is shared by the bar.

Through this method, the system can measure the displacement up to 200mm. Sensitivity is

6 nm/200mm = 0.03 nm/mm.
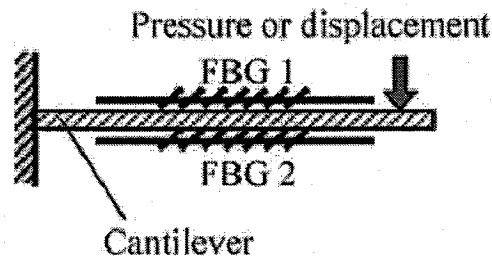
Fig.1.4 A differential fiber Bragg grating (FBG) sensor with a triangle cantilever
structure for high-pressure (or displacement) measurement[24]

Other examples [24] are the FBG element bonded onto a cantilever beam as shown

in Fig.1.4. Yong Zhao demonstrated a differential fiber Bragg grating (FBG) sensor with a

triangle cantilever structure for high-pressure (or displacement) measurement. When the

pressure changes (or displacement) makes the cantilever a bending motion, two FBGs

with the same Bragg center wavelength bonded on the upper and lower surfaces of the

cantilever are also bent, one is stretched and another is compressed, modulating the

wavelength shift in opposite directions. Displacement measurement sensitivity is ～ 1:75

pm/ μm.

Wenghong Yu[25] demonstrated a similar FBG displacement sensor, whose

measured sensitivity is 0.1051 nm/mm within the working range of –18 to + 18mm.

Weigang Zhang[26] demonstrated an FBG-type sensor for simultaneous measurement of force (or displacement) and temperature based on the bilateral cantilever beam(BCB) as shown in Fig.1.5. The two parts of the beam are subject to opposite forces (or displacements) leading to a red shift for the part of the FBG subject to stretch and to a
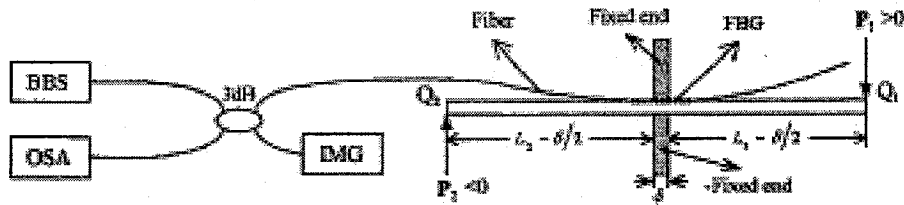
Fig.1.5. Schematic diagram of FBG –type sensor based on BCB[26]

blue shift for the other one. An FBG bonded to the surface of the middle of the BCB is experimentally demonstrated to have a force sensitivity of 1.046 nm/N, a sensitivity of the displacement-based strain of 0.317 nm/mm.

Past reports more concern about the measurement scale in range of 0.1-1mm or more. The elongation of a FBG fiber reaches the scale in mm it needs more than 300mm long. Such a large size is not always acceptable as a sensor for measuring displacement. The small absolute elongation limits FBG as a displacement sensor. In this thesis we focused on the fine displacement.

1.4 Background of Surface Measurement Instrumentation

There are two modes of surface measurement instrument in the scale of micron or submicron: contact and non-contact. The contact allows a surface to be touched using a diamond probe, stylus or indenter. The non-contact is using light or other beam. The advantages of surface measurement using a light are the absence of contact, higher

measurement speed, higher lateral resolution and greater depth range. Surface measurement using a diamond probe produces far better depth resolution and reliability, and also can be used to obtain other mechanical properties, like microhardness and modulus.

1.4.1   Surface Profiler and Step Height Measurement

A surface profiler or profilometry is used to measure the topography of a material surface.

Determining:

- the surface roughness and waviness;

- the shape and dimensions of objects;

- the thickness of coatings, paint layers and coatings;

- step height measurements in semiconductor fabrication;

- the etch depth;

- wear scar measurements

The operation is very simple. Once the sample is loaded on the stage a stylus is lowered and with a set pressure (force) the stylus scans the surface of the sample literally 'feeling' the surface to determine the surface morphology.

1.4.2   Description of Microhardness Technique

Microhardness testing is an indentation method for measuring the hardness of a material on a microscopic scale. A diamond probe, or indenter, is impressed into the material at loads from 15 to 1000 gf. The hardness H as a measure of material resistance to

irreversible deformation is then calculated as $H = F_{sub}/A$. The impression length, measured microscopically and turned into area A, and the applied load F_{sub} are used to calculate a hardness value.

The indentations are made using a square-based pyramid indenter (Vickers hardness scale) or an elongated, rhombohedral-shaped indenter (Knoop hardness scale). The hardness impressions after indentation can be precisely located with the microscope or scanning electron microscopy (SEM) and scanning force microscopy [27,28] to perform tests on microscopic features. The hardness values obtained are useful as an indicator of materials properties and expected service behavior. Conversions from microhardness values to tensile strength and other hardness scales (e.g. Rockwell) are available for many metals and alloys.

This conventional hardness test based on measurement of the impression in the surface formed by the indenter is not possible in materials when significant elastic recovery occurs [29].

1.4.3 Indentation Measurement

Indentation was initially created as a means of quality control during metallurgical processing. Recently, indentation is used for the determination of mechanical properties [1, 30], such as hardness [30,31], elastic modulus [32,33], the fracture toughness [34], surface stress [35,36,37], indentation Creep and the interfacial adhesion of films, can be measured on almost any type of material: soft, hard, brittle or ductile [38,39,40,41,42,43].

According to the international standard ISO 14577 (1), 2002, produced by the International Organization for Standardization (ISO), determination of properties based on indentation measurement [44] can be divided into three ranges (the indentation can be

controlled either in force, F_{sub}, or in depth, h_{dep}):

- Macro range: $2\,N < F_{sub} < 30\,kN$

- Micro range: $2\,N > F_{sub}$; $h_{dep} > 200\,nm$

- Nano range: $h_{dep} < 200\,nm$

According to the ranges, the measurement method studied in this thesis is in the micro range, and it has the possibility down to the nano range if Bragg grating sensor and the optical spectrum analyzer are improved.

An advantage of the indentation measurement comes from the fact that the using the force-depth data to determine mechanical properties without an additional observation on the hardness impression as the microhardness measurement does.

The operating principle of the indentation instrument is as follows: An indenter tip, normal to the sample surface, is driven into the sample by applying an increasing load up to some preset value. The load is then gradually decreased until partial or complete relaxation of the material. From the test, a typical load-depth curve can be drawn and the material properties can be obtained by analyzing the curve.

Fig.1.16 gives a schematic representation of typical load-depth curves. A loading curve records the elastic and plastic deformation of a sample. The unloading curve can be considered as just containing the elastic deformation. The unloading process shows different cases of response on the unloading curves. For pure elastic material, there is no plastic and the unloading curve is almost the same as the loading curve because the geometry of the deformation is almost completely reversible.

For the elastoplastic or rigid-plastic material, the unloading curve is different from

the loading curve. If rigid-plastic material can be considered as no elastic component, the
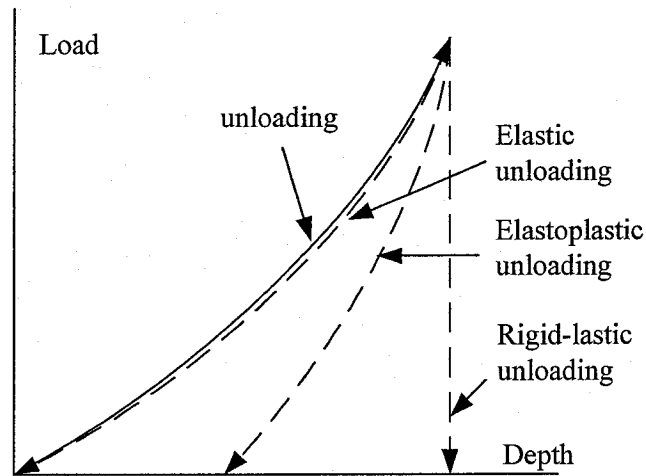
Fig. 1. 6. Typical load-depth curves[45]. The solid line
is loading curve. There are three typical unloading
curves for different materials
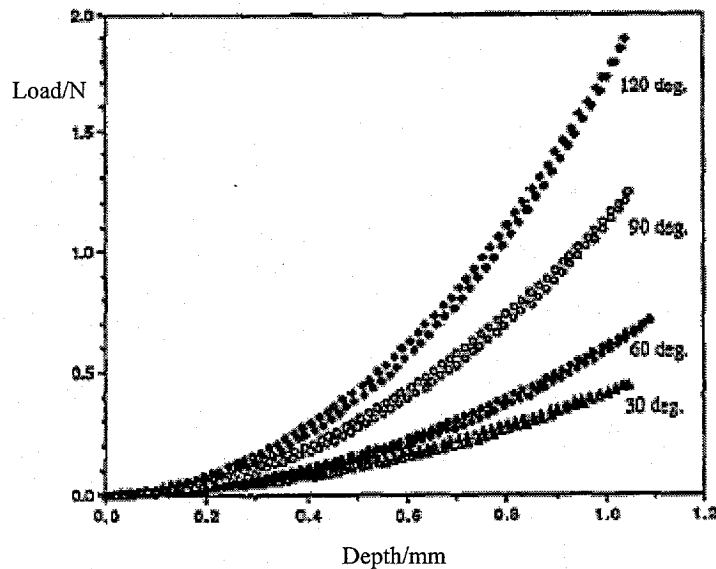
Fig. 1. 7. Load-depth data for an elastic material sample
indented by cones of various included angles[45].

deformation is completely irreversible. An elastic material example was carried out by B J

Briscoe [45] shown in Fig.1.7. In his experiment, poly(isObutadiene) rubber was indented by

14

cones of various included angles. The range of the load was within a 0-20 N load. The displacement range can reach more than 3mm. Two curves are shown for each data set; the upper curve is the loading curve and the lower curve indicates unloading. Comparing unloading curve with loading curve in the plot, it was found that the unloading process is similar to the loading curve.

The load–depth plot of an elastoplastic material example was made by Peng Gao[1] shown in Fig.1.8. In the experiment, ground and polished 6061Al alloy was used as a
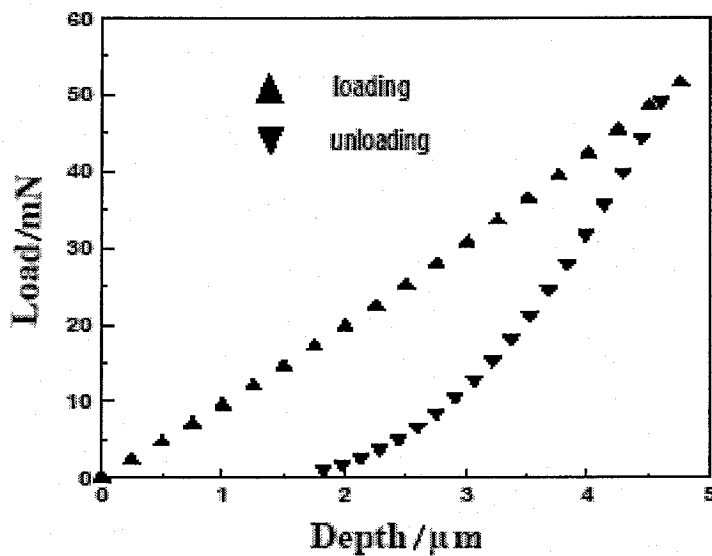
Fig.1.8. Load-depth plot for an elastoplastic material sample indented by cones of various included angles[1].
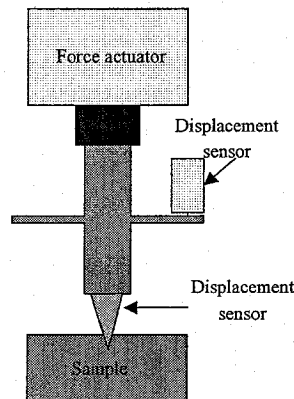
Fig.1.9. Indentation measurement system configuration

15

sample.

The indentation device consists of three basic components: an indenter mounted to a rigid column through which the force is transmitted, an actuator for applying forces and a displacement sensor for measuring the displacement of the indenter, as shown in Fig.1.9.

Indentation measurement systems are different in the ways that the force is applied and the displacement is measured. The force actuator can be generally in three forms: electromagnetic actuation, electrostatic actuation and piezoelectric actuation through springs. An schematic of the third force actuation is shown in Fig.1.10. The tip of an indenter is applied force through a spring by displacement actuator. The cantilever beam approach is the most common application of spring-based force actuation illustrated in Fig.1.11.a and b. The indenter tip attached to the free end of a cantilever beam as a spring
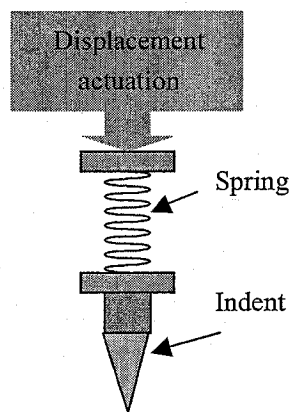
Fig. 1. 10. Indentation device using piezoelectric force actuation

is applied force by the displacement of sample driven by a piezo actuator. The indenter displacement is determined by the displacement of a laser beam reflected from the free end of the beam shown in Fig.1.11.a. Another approach of the spring-based force actuation is shown in Fig.1.11.b. In this approach, the indenter tip attached to long leaf springs is

16

applied force by the displacement of the carriage produced by a piezo actuator. The indentation application of FBG in this thesis is similar to the model shown in Fig.1.10
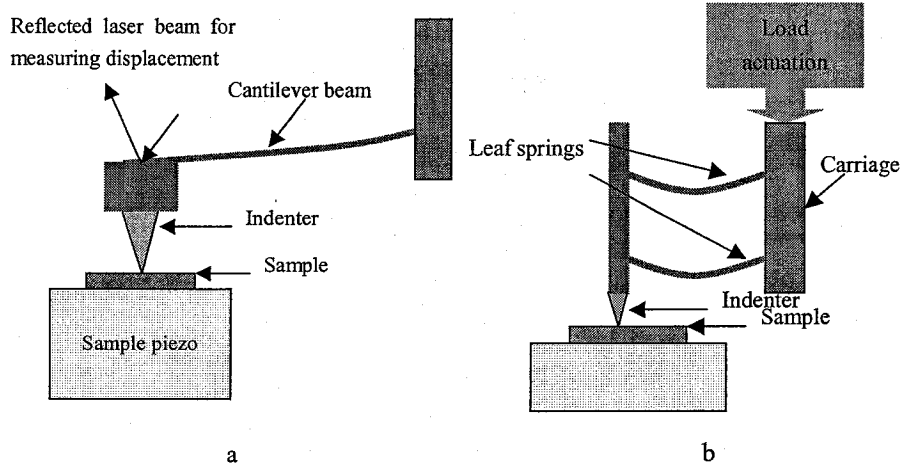
Fig. 1. 11. Two of indentation devices with the cantilever beam approach as a spring driven by the displacement of a piezo actuator.

(1) Indentation Hardness

The indentation hardness is defined as the mean contact pressure and is given by:

$$H_{IT} = \frac{F_{max}}{A_p}$$

where F_{max} is the maximum load and A_p is the projected contact area at that load.

(2) Indentation Modulus

The indentation modulus is calculated from the slope of the tangent of the unloading curve, whether using a linear fit to the initial unloading data or a power-law fit [4]:

$$E_{IT} = \frac{1 - v_s^2}{\frac{1}{E_r} - \frac{1 - v_i^2}{E_i}}$$

where E_i is the elastic modulus of the indenter (1141 GPa for diamond), v_i is the Poisson's

17

ratio of the indenter (0.07 for diamond) and v_s is the Poisson's ratio of the tested sample. The reduced modulus, E_r, which is calculated from the indentation data is defined as:

$$E_r = \frac{\sqrt{\pi} \cdot S}{2 \cdot \beta \cdot \sqrt{A_p(h_c)}}$$

(3) Indentation Creep

Indentation creep measurement tests the time-dependent mechanical response of a material [46]. The indentation creep can be defined as the relative change of the indentation depth depending on time whilst the applied load remains constant.

1.5 Scope of the Thesis

The purpose of this thesis is to establish a new methodology in the characterization of material surface by using the Bragg grating fiber technology reaching into micro scale or sub-micrometer scale. To achieve fine displacement measurement and to monitor and control the force applied to the substrate are the two themes that run through the whole thesis.

In general, the thesis is divided into three sections.

The first section of the thesis includes Chapter 1 where an overview of fiber optic sensor technology is presented, and the technology background related to the thesis is introduced.

The second section is the core part of thesis, which composes of Chapter 2 through Chapter 4. Entire theoretical and experimental progresses made are presented in this section. Chapter 2 presents theories used in the thesis. The formulas for the reflective wavelength shift caused by strain are remarked in new significance in displacement and force for the fine surface measurement application. The displacement measurement

18

sensitivity, measurement range and the force to the substrate are analyzed in the section. Suggestions to improve the sensitivity are proposed. One FBG indentation measurement is proposed and theoretically analyzed. To drive the sensing probe smoothly up and down and to monitor and control the force against the sample, an additional grating is introduced to form a two-grating measurement system. The theory on displacement sensing and force monitor grating measurement system is derived. Used the monitor grating fiber, the load weight against the substrate and the deformation of the substrate surface can be monitored and controlled. The indentation measurement using two gratings is theoretically proposed. In Chapter 3, preparation work and experimental set-up are presented. The behavior of FBG fiber is investigated through three fundamental kinds of long FBG fiber experiments. Experiments in this chapter expect the feasibility and practicality of the fine displacement and force measurement. Experiments directly give the proof that the characteristic shift of the reflected wavelength can be produced by an elongation of grating fiber or by an applied load force. Experiments reported in the chapter follows theoretical laws well. Furthermore, in this chapter some other preparative work are reported. The set-up of fine surface measurement system is demonstrated. Finite element model in the ANSYS environment is used to model and simulate the deformation at the interface between the ruby probe and the surface of the silicon wafer. The deformation of the surface is an important factor that may influence the step height measurement and may provide physical information about the surface material, but how the deformation gives material information is out of the thesis scope. This Chapter also describes the preparation of step samples, which are made to be step height standards to test the measurement system and are checked and measured by the scanning electron microscope (SEM). Chapter 4 presents the experimental results and

discussions. The experiments of one grating indentation measurement, two grating indentation measurement and the step height measurement are reported in the chapter. The experimental deformation is compared with simulation results. Other experimental investigations are reported.

Chapter 5 covers the summary, conclusion, contribution and suggested future work.

CHAPTER II

THEORY ON FINE DISPLACEMENT AND FORCE SENSING

SYSTEM

The theory on the fine measurement system by using fiber Bragg grating (FBG) is discussed in this chapter. First part of this Chapter is on the one-grating system including a dual grating array system, while the second part is on the two-grating system.

2.1 One-grating Fine Measurement

2.1.1 Relation between Strain and Shift of the Reflected Wavelength

The displacement measurement by using FBG is based on the strain effect on FBG introducing a shift in the characteristic transmission or reflection wavelength as mentioned in Chapter I. Injecting light from a spectral broadband source into a fiber with a Bragg grating, a narrowband spectral component at the Bragg wavelength is reflected by the grating, and in the transmitted light this spectral component is missing. The reason for this phenomenon is that under the phase matching conditions, a fiber Bragg grating (FBG) couples the forward propagating core mode to the backward propagating core mode. In a FBG the Bragg wavelength λ_B, or the central wavelength of the reflected light, is given by[47,48,49]

$$\lambda_B = 2n_{eff}\Lambda \tag{2.1}$$

where n_{eff} is the effective refractive index of the fiber core and Λ is the grating period. In Eq. (2.1) it can be seen that the Bragg wavelength can be changed with respect to a change in the grating period or the effective refractive index. A shift in the Bragg wavelength of the grating in either the reflected or transmitted spectrum can be used to detect strain and temperature that result in the perturbation of the grating. The strain response arises due to

both the physical elongation of the sensor (and corresponding fractional change in grating pitch) and the change in fiber index due to photoelastic effects, whereas the thermal response arises due to the inherent thermal expansion of the fiber material and the temperature dependence of the refractive index.

The shift in Bragg wavelength, $\Delta\lambda_B$ in the unit of nm, with strain ε ($\varepsilon=\Delta l/l$, the longitudinal deformation of the fiber normalized by the length of fiber, in the unit of $\mu\varepsilon$) and temperature T in the unit of °C can be expressed using

$$\Delta\lambda_B = K_\varepsilon\Delta\varepsilon + K_T\Delta T \tag{2.2}$$

where K_ε and K_T are coefficients in the units of nm/ $\mu\varepsilon$ and nm/°C, respectively. For one FBG at the constant temperature, $\Delta T\approx0$, (2.2): $\Delta\lambda_B = K_\varepsilon\Delta\varepsilon$. The relation $\Delta\lambda_B$ to ε can expressed by[47,48,49,50]

$$\Delta\lambda_B = \lambda_B\,(1\text{-}p_e)\varepsilon \tag{2.3}$$

where $p_e{}^t$ is the effective photoelastic constant[48].

For 1550nm grating, the measured strain response at constant temperature can be

$$\Delta\lambda_B = 1.2\times10^{-3}\varepsilon \tag{2.4}$$

where $\Delta\lambda_B$ is in nm and ε in $\mu\varepsilon$ ($\mu\varepsilon$=microstrain). Near the Bragg wavelength of 830 nm, the typical response of the Bragg wavelength shift to strain is~0 .64 pm /μ ε, and ~1pm/μ ε near 1300 nm.

The thermal response in constant strain condition is

$$\Delta\lambda_B = 2\left(\Lambda\frac{\partial n_{eff}}{\partial T} + n_{eff}\frac{\partial\Lambda}{\partial T}\right)\Delta T$$

---

[t] The effective photoelastic constant p_e is in terms of the fiber Pockel's coefficients p_{ij} and the Poisson ratio μ:

$$= \lambda_B(\alpha + \zeta)\Delta T \tag{2.5}$$

For 1550nm grating, a typical value for the thermal response is 0.01 pm/°C[48].

2.1.2 Principle of Displacement Fiber Bragg Grating Sensor

From equation (2.3) we can get

$$\Delta \lambda_B = \lambda_B (1 - p_e) \frac{\Delta l}{l} \tag{2.6}$$

Or for 1550nm grating,

$$\Delta \lambda_B = 1200 \frac{\Delta l}{l} \tag{2.7}$$

where $\Delta \lambda_B$ is in nm. l and Δl is the length of the fiber and the fiber length change respectively. It indicates that when l, the length of sensing part of the fiber in which there is a Bragg grating, makes an expansive change Δl and becomes the length of $l + \Delta l$, the reflected wavelength of the grating shifts $\Delta \lambda_B$ and becomes $\lambda_B + \Delta \lambda_B$ from λ_B. If one end, A, of the fiber is fixed, the elongation of the fiber can be made by the other end moving from B to B' as shown in Fig.2.1.

$$p_e = \frac{n_{eff}^2}{2}\left[p_{12} - \mu(p_{11} + p_{12})\right].$$
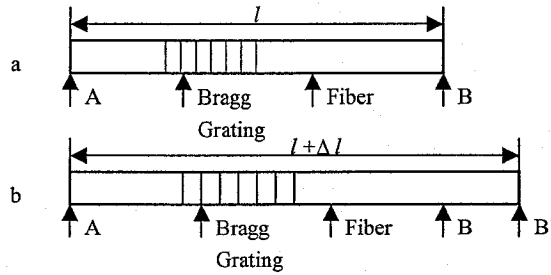
Fig. 2.1. A fiber is stretched Δl from a) the length l to b) the length $l + \Delta l$. When the end A is fixed, the anther end will change from B to B' .

The reflected wavelength shift responses the length change of grating fiber. When an end of the fiber is fixed, a displacement of another end can be detected by a shift of characteristic reflected wavelength from a Bragg grating, which is the basic operation of a FBG based sensor system for displacement measurement.

2.1.3　Vertical Displacement Measurement with a Load

When a fiber with a grating is hung in the air and the top end of fiber is fixed, another end (the bottom end) is changeable and could be changed into positions as shown in Fig2.2. The highest position is related to no load situation. The lowest position is related
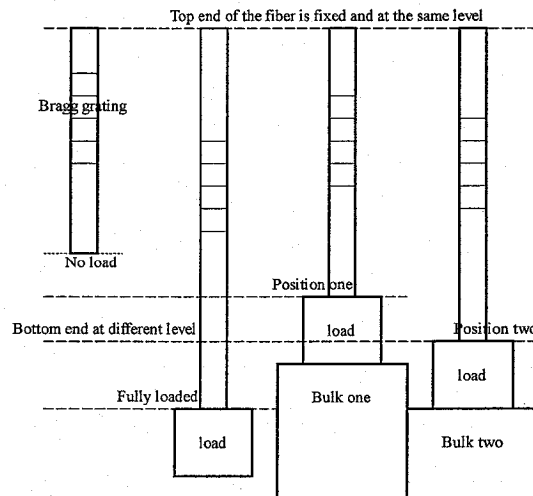
Fig. 2.2 A fiber changes its length as the bottom end of the fiber changes its positions when the top of the fiber is fixed.

24

to the grating fiber fully loaded by a load W. The position 1 is related to the load on a higher bulk, and the position 2 is related to the load on a lower bulk.

The characteristic wavelength of a grating fiber shifts with respective to the changes of the fiber length. Consequently, different positions produce different length of fiber and lead to different reflected wavelength(Chapter 3 has experimentally checked this property).

Without load, there is no force against the grating fiber and the bottom end of the fiber is at highest position. If W is the weight of the load, when W is fully loaded under the fiber, causes the fiber stretches downward.

From equation (2.7),

$$\lambda_B - \lambda_0 = 1200 \frac{l_f - l_0}{l_0} \tag{2.8}$$

Where λ_0 and λ_f, are the reflected wavelengths in the unloaded and fully loaded conditions respectively as shown in Fig.; l_0 and l_f are the lengths of fiber unloaded and fully loaded, respectively.

When put the load on a higher bulk, the bottom of the fiber is at position 1, as shown in Fig.2.2. And then

$$\lambda_m - \lambda_1 = 1200 \frac{l_m - l_1}{l_0} \tag{2.9}$$

25

$$\lambda_1 - \lambda_0 = 1200 \frac{l_1 - l_0}{l_0}$$

(2.10)

where λ_1, l_1 are the reflected wavelength and the length of the fiber with respect to the bottom end of fiber at position 1, respectively.

Similarly, the load on a lower bulk makes the bottom of the fiber at position 2, as shown in Fig.2.2, we can obtain the relation between λ_2 and l_2 and then find

$$\lambda_2 - \lambda_1 = 1200 \frac{l_2 - l_1}{l_0}$$

(2.11)

The reflected wavelength positions λ_0, λ_m, λ_1 and λ_2 with respect to the four positions of the bottom end of the fiber are shown in Fig.2.3. In Fig.2.3, we can see $\Delta\lambda = \lambda_2$
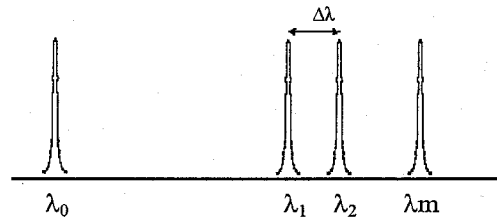
Fig 2.3 Reflection wavelength shifts from no strain state of λ_0 to the state of λ_m with a load, and to the position 1 of λ_1 and then the position 2 of λ_2.

- λ_1 is the wavelength difference between two reflection wavelengths at position 1 and at position 2. From the equation (2.11), it is known that a change of FBG reflection wavelengths is proportional to a displacement from one position to another.

If neglect the deformation of the sample surface when the probe is touching, this displacement measurement method can be applied to measure the surface topography, such as step height measurement that can be illustrated in Fig.2.4. When the top end of the FBG fiber doesn't change and the substrate level vertically changes, the load and probe under the bottom end of the grating fiber also move from one height to another, which causes fiber to elongate and the reflected wavelength to shift. Measuring the shift of the peak of the reflection spectrum will result the step height or topographic feature of sample surface.
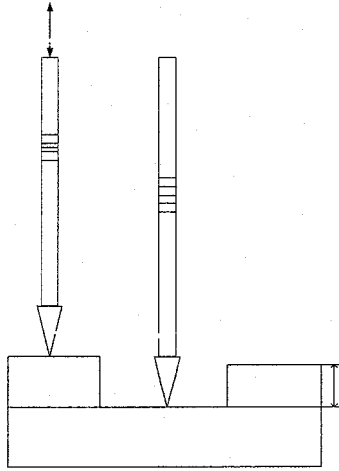
Fig2.4 An ideal layer thickness measurement without sample deformation

From Eq.(2.11) it is known

$$l_2 - l_1 = \frac{l_0}{\lambda_B(1-p_e)}(\lambda_2 - \lambda_1)$$

(2.12)

For 1550nm grating,

$$l_2 - l_1 = \frac{l_0}{1200}(\lambda_2 - \lambda_1) = 8.33 \times 10^{-4} l_0(\lambda_2 - \lambda_1)$$

(2.13)

Where λ_1 and λ_2 are in nm, l_1, l_2 and l_0 are in the same unit. If we know λ_1 and λ_2 we can calculate the step height (l_2-l_1).

2.1.4 The Range of the Displacement Measurement

The range of this displacement measurement system is the distance from the unloaded position to the fully loaded position, i.e $(l_m - l_0)$ because the length of the sensing FBG fiber can only change from l_0 to l_m. The displacement range is dependent on the weight, W, of the load that we used. Without load, there is no force against the grating fiber and the bottom end of the fiber is at highest position. When no substrate supports the load and probe, the FBG is fully loaded by the load (W is the weight of the load) and the bottom end of the fiber is at lowest position.

Thus, the load weight determines the range of the displacement system.

2.1.5 Displacement Sensitivity

From Eq. (2.12),

$$\Delta \lambda = \frac{\lambda_B (1 - p_e)}{l}(l_2 - l_1)$$

(2.14)

$\dfrac{d\lambda}{dl} = \dfrac{\lambda_B (1 - p_e)}{l}$ can be defined as the measurement sensitivity because it describes how sensitive the sensor is when it responses to a unit displacement.

The sensitivity is an important factor for fine displacement measurement by using FBG due to two reasons: one is that for limited resolution of the optical spectrum analyzer (OSA), higher sensitivity means the sensor can detect smaller displacement, and can detect the displacement that the sensor with lower sensitivity can't. Another reason is that the sensor with bigger sensitivity can obtain more accurate result for measuring the same displacement value of $(l_2 - l_1)$ compared to the sensor with smaller sensitivity.

2.1.6 Improvement of the Sensitivity

The sensitivity improvement raises the detection power and measured reliability for

28

the fine displacement measurement.

From Eq.(2.14), for a certain value of displacement of $(l_2- l_1)$, in order to obtain larger value of $\Delta\lambda_B$, in the right side of Eq 2.14 either the denominator should be small or the nominator should be large. Thus, to improve the displacement sensitivity l should be small, while λ_B and $(1-p_e)$ should be large.

2.1.7   Displacement Sensor Using a Dual Grating Array

To raise the sensitivity, a dual-grating array displacement measurement method is proposed in this work. There are two advantages using this method. It doubles the sensitivity and the device is temperature independent.

As shown in Fig 2.5, two FBGs are imprinted close to each other in a serial arrangement in the same fiber. The two-FBG fiber is stretched when mounted. The moving
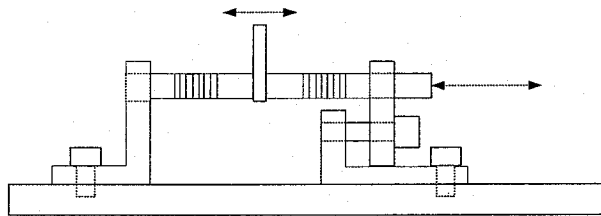
Fig. 2. 5 Temperature independent displacement sensor

part is fixed at the middle place between two gratings.

To understand how the dual grating works, first we assume that the two gratings have the same characteristics. Reflected wavelengths of two FBG fibers without strain are the same value of λ_B, those reflected wavelengths are overlapped as shown in Fig. 2.6.a. When the fiber of two FBGs are stretched, their reflection wavelengths shift to the same value of $(\lambda_B +\Delta\lambda_B)$ because from equations (2.2) and (2.3) two gratings have the same $\Delta\lambda_B$

29
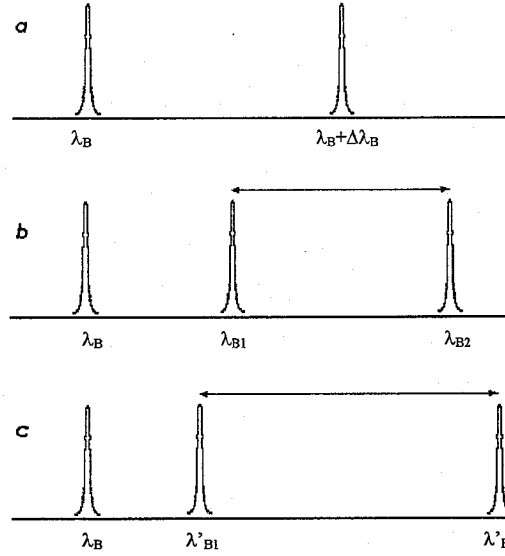
Fig. 2.6 Reflected wavelengths shift for two same gratings a) as Moving part is at centre b) as moving part moves at position 1 from the centre c) as moving part moves at another position from the position 2.

$= \lambda_B(1-pe)\varepsilon + \lambda_B K_T \Delta T$, as illustrated as the peak at $(\lambda_B + \Delta\lambda_B)$ in Fig. 6.a. The strain of the fiber ε is the same for two gratings when the fiber is stretched.

When the moving part between two gratings moves to a position called position 1, the peaks of two reflected wavelengths are separated, for a grating to λ_{B1} and for another grating to λ_{B2} because they feels different strain as shown in Fig.6.b, and according to the equation (2.2), the shift from original λ_B to λ_{B1} and to λ_{B2} respectively for two gratings are different:

$$\lambda_{B1} - \lambda_B = \lambda_B(1-pe)(\varepsilon-\Delta\varepsilon) + \lambda_B K_T \Delta T \qquad (2.15)$$

$$\lambda_{B2} - \lambda_B = \lambda_B(1-pe)(\varepsilon+\Delta\varepsilon) + \lambda_B K_T \Delta T \qquad (2.16)$$

Subtracting (2.15) from (2.16) results

$$\lambda_{B2} - \lambda_{B1} = 2\lambda_B(1-pe)\Delta\varepsilon \qquad (2.17)$$

where $\Delta\varepsilon$ is produced by the moving part from the stretched position to the position 1, λ_{B2} and λ_{B1} are the two gratings' reflected wavelengths at the position 1. From (2.17), we know

that the difference $(\lambda_{B2} - \lambda_{B1})$ of the reflected wavelengths is independent of the temperature because the temperature factor has been cancelled.

If the distance between the stretched position and position 1 is Δl, and at the beginning the moving part is at the middle between two gratings $l_1 = l_2 = l$, so $\Delta\varepsilon = \Delta l / l$. (2.17):

$$\lambda_{B2} - \lambda_{B1} = 2\lambda_B(1\text{-pe})\, \Delta l / l \qquad (2.18)$$

Comparing (2.18) with (2.6), we see that the sensitivity is doubled.

The moving part moves from the position 1 to another position called position 2 as shown in Fig.2.6.c. λ_{B2}' and λ_{B1}' are the two gratings' reflected wavelengths at the position 2. If $\Delta\lambda = (\lambda_{B2}' - \lambda_{B1}') - (\lambda_{B2} - \lambda_{B1})$ is the subtraction between the two differences of the two wavelengths at the two positions.

$$\Delta\lambda = 2\lambda_B(1\text{-}p_e)\, \Delta l / l \qquad (2.19)$$

where Δl is the distance between two positions at which the moving part are located, and one of position could be the unmoved position. For example for 1550nm grating, the length of each FBG fiber is ~5 mm (between them there is the moving part), and a distance between position 1 and position 2 is $0.1\mu m$ causes $\Delta\lambda = 0.048nm$. As we has discussed before, this value should be created in a single grating system for moving $0.2\mu m$. Compared to a single grating system, the dual grating array system provides more capability to measure smaller displacement because the sensitivity is improved.

In short, in the proposed dual-grating system, the moving part moves from one position to another position causes the wavelengths of the two gratings to be separated in opposite directions. A change of the difference between two wavelengths from two gratings at different positions is proportional to a displacement of the moving part from one

position to another. This dual-grating system doubles the sensitivity, an important factor for the fine displacement, and is also temperature independent.

2.1.8   Relation between Force and Sample Position

According to Hooke's law for linear elastic material,

$$F = E \cdot A \cdot \varepsilon = E \cdot A \cdot \Delta l / l \tag{2.20}$$

where F is the force against the fiber, E is the elastic modulus or young's modulus, A is the cross sectional area of the fiber, $\varepsilon = \Delta l / l$ is the strain. From this equation, we know that a bigger force F is applied against the fiber causes a longer elongation Δl of the fiber.

There are three conditions should analyzed. The first is no load, the second is the grating fiber is fully loaded by a load without a sample support. The third is grating fiber is loaded by a load with a sample support.

No load pushes the grating, $F = 0$ in the first condition; When the grating fiber is fully loaded by a load W without a sample support. The force against the grating fiber is the biggest and is equate to W. If W is the weight of the load, the biggest force against the fiber is W. If the load W doesn't touch a sample, $F = W$, Eq.(2.20):

$$W = E \cdot A \cdot (l_m - l_0) / l_0 \tag{2.21}$$

where l_0 and l_m are the lengths of the fiber when the fiber is unloaded and fully loaded by a load, respectively.

In second condition, at a position in the range from l_0 to l_m, there is a sample supporting the load. If a length change of the fiber from l_0 to l, the force against fiber is depended on $(l-l_0)$, the distance from the position to the unload position.

$$F = E \cdot A \cdot (l-l_0) / l_0 \tag{2.22}$$

$$F = \pi \, E \, r^2 \cdot (l-l_0) / l_0 \tag{2.23}$$

32

Where r is fiber's radius, $A = \pi r^2$. Since a typical force bearing cross sectional areas is 0.0123 mm^2, and the elastic modulus of fiber is 72900N/mm^2[22,51,52] for 1550nm grating the force against fiber is

$$F=9.3\times10^4(l-l_0)/\ l_0 \qquad (2.24)$$

The force against substrate offered by the object of load and probe can be expressed by

$$F_{sub}=\pi E\ r^2(\ l_m - l)\ /\ l_0 \qquad (2.25)$$

Eq.(2.25) can be derived in the following consideration. When we consider the load and probe as an object, there is three forces against the object of load and probe. The weight force W comes from gravity, a force F comes from grating fiber, and a force F_{sub} comes from sample. Because the object of load and probe is in stationary, $W = F_{sub} + F$. The force F come from grating fiber is equal to the force offered by the load and probe, so F can be expressed by (2.22). From the expressions of (2.21) and (2.22) we obtain the Eq.(2.25).

From Eq.(2.22) and (2.25),The force against fiber is dependent on the distance from the position to the unload position, and the force against sample is dependent on the distance from the position to the fully loaded position. From Eq.(2.21), we know that the weight of load and the probe, W, determines the displacement measurement range of (l_m-l_0). Large W causes longer displacement measurement range.

2.1.9 Relation between Force and Reflected Wavelength

We also can find the relation between the force against fiber and the shift of the characteristic wavelength and find the relation between the force against the substrate and the shift of the characteristic wavelength.

The relation between the force against fiber and the shift of the characteristic wavelength could be

$$\Delta\lambda_B = \lambda_B(1-p_e)\frac{\Delta l}{l} = \lambda_B(1-p_e)\frac{F}{EA} \tag{2.26}$$

A is approximately $0.0123mm^2$. $E=72900N/mm^2=73GPa$[22,51,52]. The equation represents the change in the wavelength reflected by the FBG with respect to the stretching force of load or weights. The Young modulus of the transducer is used in order to obtain the strain from the applied force.

For λ_B=1550nm grating fiber,

$$\Delta\lambda_B = 1.33\times10^{-2}F. \tag{2.27}$$

where unit of F is gram or gf and $\Delta\lambda_B$ in nm.

$$F = \frac{EA}{\lambda_0(1-p_e)}(\lambda-\lambda_0) \tag{2.28}$$

For λ_B=1550nm grating fiber,

$$F = 75.2(\lambda-\lambda_0) \tag{2.29}$$

where unit of F is gram or gf and $\Delta\lambda_B$ in nm. The force against grating fiber can be known from the characteristic wavelength shift.

Similarly, the force against the substrate can be expressed by

$$F_{sub} = W - \frac{EA}{\lambda_B(1-p_e)}(\lambda-\lambda_0) \tag{2.30}$$

$$F = \frac{EA}{\lambda_B(1-p_e)}(\lambda_m-\lambda) \tag{2.31}$$

or for 1550nm grating fiber

$$F = 75.2(\lambda_m-\lambda). \tag{2.32}$$

where unit of F is gram or gf and $\Delta\lambda_B$ in nm.

2.1.10 Force Sensitivity

We rewrite (2.26) here,

$$\Delta\lambda_B = \frac{\lambda_B(1-p_e)}{EA}F$$

(2.27)

$\dfrac{d\lambda}{dF} = \dfrac{\lambda_B(1-p_e)}{EA}$ is defined as the force sensitivity. Enhancing the force sensitivity

can reduce the force against sample and produce less deformation of the sample. The

improvement of the force sensitivity can be achieved by reducing the diameter of fiber

using etching method.

2.1.11 Indentation Application Using One Grating

A simple indentation measurement using one FBG is proposed here. This

indentation measurement may work in compressive and tensional ways shown in Fig.2.7.
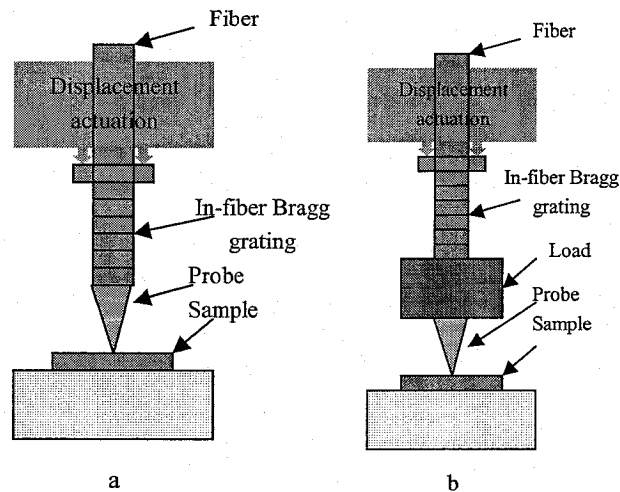
Fig.2.7. Schematic of two proposed indentation measurement using one FBG fiber

35

The proposed indentation in compressive way, shown in Fig.2.7.a, consists of one grating, a probe and a displacement actuator. When it works and the probe indents into the sample, the FBG is compressed. The proposed indentation in tensional way, shown in Fig.2.7.b, consists of one grating, a probe, a displacement actuator and a load. The FBG is stretched by the load when it works. The purpose of displacement actuation is to make relative movement between a sample and the top end of the FBG fiber, so two methods can realize the purpose: 1) the sample is fixed and the top end of the FBG fiber moves; 2) the tope end of the FBG fiber is fixed and the sample moves. Fig.2.7.a and b show the displacement actuation at the top end of the FBG fiber, but the experiment presents in thesis is from the sample driven by stages. Controlling the displacement of the top end of the FBG fiber or a sample, the relative movement between the top end of the FBG fiber and the sample applies different forces through the probe to the sample and produces the different depth of
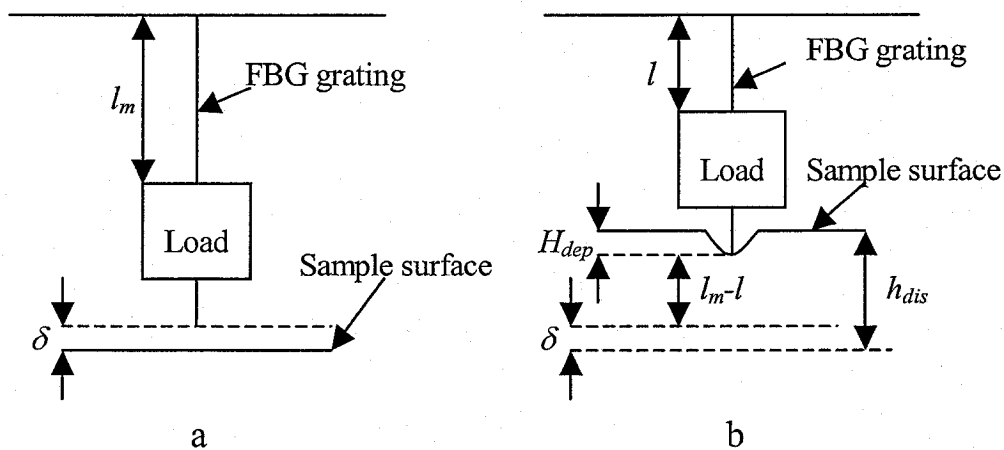
Fig. 2. 8. Operation of an indentation measurement using FBG. a) surface of sample is not reached to probe; b) the probe has indented into the sample.

probe into the sample. In this thesis only the tensional indentation is investigated.

The operation of this tensional indentation measurement can be described in Fig.2.8.a and b. At the beginning, the FBG fiber is fully loaded by a load and the probe

doesn't touch the surface of sample shown in Fig2.8.a. When the top end of the FBG fiber is lowered down or the sample is raised up, the probe will contact with the sample and indent into the sample shown in Fig.2.8.b. In the experiment, the sample is moved by a positioner (a stage) and the top end of the FBG fiber is fixed. The above discussion is also suitable for the movement case of the top end of the FBG fiber that also can make the relative movement between the indenter and the sample. From the Fig.2.8.b, the relation between the depth of the probe into the substrate and the shift of reflected wavelength can be expressed by

$$h_{dep} = h_{dis} - \delta - (l_m - l) \tag{2.28}$$

where h_{dep}, h_{dis} δ, l_m and l are the depth of the probe into the sample or deformation of the material surface, the displacement of sample approaching to the probe, the offset, the length of the FBG fiber as it is fully loaded and the length of the FBG fiber after the sample displacement has be made. $(h_{dis} - \delta)$ is the part of the sample displacement after probe has indented into the surface of the sample. Using the relation $\Delta\lambda = \dfrac{\lambda_B(1-p_e)}{l}(l_2 - l_1)$, we have

$$h_{dep} = h_{dis} - \delta - (l_m - l) = h_{dis} - \delta - \frac{l_0}{\lambda_0(1-p_e)}(\lambda_m - \lambda) \tag{2.29}$$

The force against substrate may be

$$F_{sub} = \frac{EA}{\lambda_0(1-p_e)}(\lambda_m - \lambda) \tag{2.30}$$

In experiment, choosing different displacements h_{dis} of the sample and measuring the reflected wavelength λ, we can draw a curve of sample's displacement h_{dis} versus reflected wavelength λ from the grating. Based on this relation between h_{dis} and λ, we can

obtain the force-depth curve from the above two equations and then use this force-depth curve we can analyze the mechanical property of the material of the sample as the ordinary indentation measurement does.

2.1.12 Discussion on One Grating System

One FBG fiber can sense the displacement and sense the applied force against the substrate as well. Theoretically the proposed fine displacement sensing method could be used to measure a fine displacement in the micron scale or below. Meanwhile, the forces against the fiber and against the sample can also be monitored by the reflected wavelengths from the same grating fiber. The indentation measurement using one grating is a good example as its application.

2.2 Theory on Two Grating Measurement System

In order to control and move the load and probe smoothly up and down and in order to monitor and control the force against the sample separately from sensing displacement, an additional grating fiber is introduced to form a measurement system consisted of a displacement sensing grating and a force monitor grating. In the thesis, the displacement sensing grating fiber is called S grating fiber, the force monitor grating fiber is called M grating fiber.

The set-up of the displacement sensing and monitor grating measurement system is shown in Fig.2.9. Two grating fibers are connected to the load. The bottom end of M grating fiber is placed at the same location at the center of the top of the load as S grating
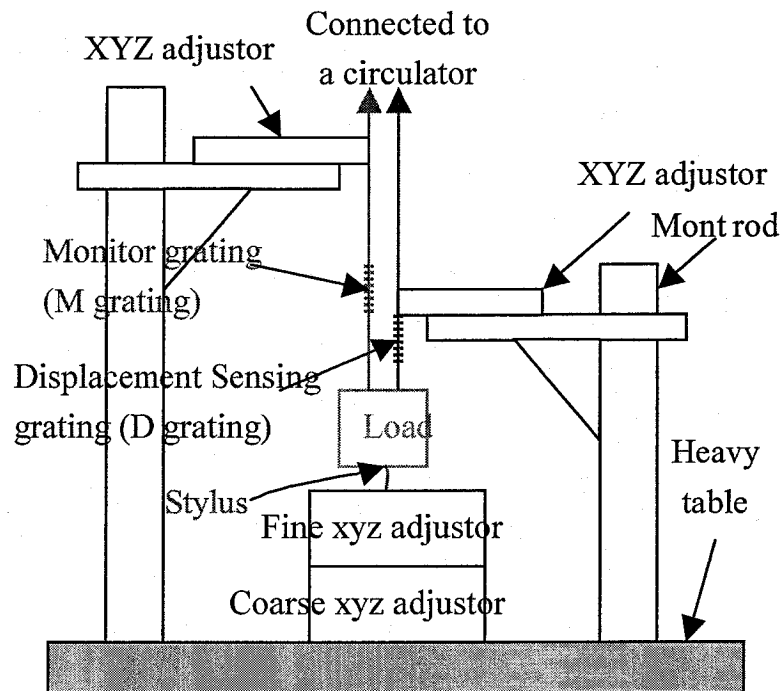
Fig. 2. 9. The set-up of the sensing and monitor grating measurement system

fiber does. Unlike the S grating fiber whose top end is fixed, the top end of M grating fiber is movable and can be driven up and down by an adjuster.

2.2.1 Operation of the displacement sensing and Monitor Gratings

Fig.2.10. can be used to describe how the two-grating system works. As the top end of M grating fiber is adjusted to be down (or up), it drives the load down (or up).

39

In Fig.2.10.a, the top end of M fiber reaches the high position at which S grating fiber has no strain, and M grating fiber carries whole weight of the load, W. At this status a,
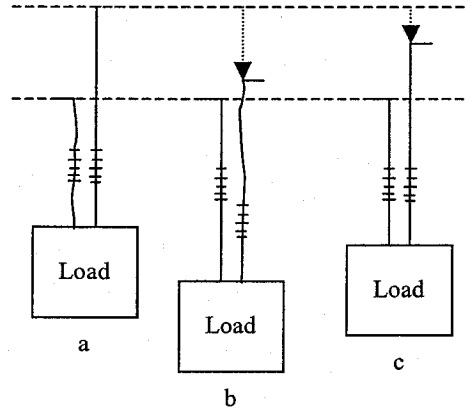
Fig.2.10. Diagram of the operation of the displacement sensing and monitor
gratings
a) The displacement sensing grating is released and the monitor grating is fully
loaded. b) The displacement sensing grating is fully loaded and the monitor
grating is released. c) Both gratings together carry the load weight.

the reflected wavelength from S grating is the shortest $\lambda_{s,min}$, related to no strain, no fiber elongation and no reflection shift i.e $\Delta\lambda_{s,min}=0$; on the contrast the reflected wavelength from M grating has its longest wavelength $\lambda_{m,max}$, related to maximum strain, fully elongated by the load and the maximum reflection shift i.e $\Delta\lambda_{m,max}$.

In Fig. 2.10.b, the top end of M fiber goes to its lowest position at which S grating fiber is fully loaded, carrying whole weight W of the load, while M grating is released with no strain. At the status b, the reflected wavelength from S grating is the longest $\lambda_{s,max}$ with the maximum reflection shift, i.e $\Delta\lambda_{s,max}$; on the contrast that from M grating reaches the shortest wavelength $\lambda_{m,min}$ with no reflection shift, i.e $\Delta\lambda_{m,min}=0$.

Between statuses of a and b, both gratings together carry the load weight. If the load

40

weight is W and M grating fiber carries the weight of $F_m = \Delta W$, S grating fiber carries the weight of $F_s = (W - \Delta W)$ because there is no sample touches the load and probe. The sum of the weights they both carry is the load weight W ($F_m + F_s = \Delta W + W - \Delta W = W$). From the status b to c, M grating fiber carries the weight from 0 to ΔW, M grating's reflected wavelength shifts ($\lambda_m - \lambda_{m,\,min}$) from $\lambda_{m,\,min}$ to λ_m, while that of S grating fiber shifts ($\lambda_s - \lambda_{s,\,max}$) from $\lambda_{s,\,max}$ to λ_s.

From the status in Fig. 2.10.a, since monitor grating fiber is fully loaded,

$$\frac{\lambda_{m,max} - \lambda_{m,min}}{\lambda_{m,min}} = \frac{(1 - p_e)W}{EA}$$

(2.31)

From status in Fig. 2.10.b, since sensing grating fiber is fully loaded,

$$\frac{\lambda_{s,max} - \lambda_{s,min}}{\lambda_{s,min}} = \frac{(1 - p_e)W}{EA},$$

(2.32)

From the last above two equations, we have

$$\frac{\lambda_{s,max}}{\lambda_{s,min}} = \frac{\lambda_{m,max}}{\lambda_{m,min}}$$

(2.33)

or $\dfrac{\lambda_{m,min}}{\lambda_{s,min}} = \dfrac{\lambda_{m,max}}{\lambda_{s,max}}$

(2.34)

From Fig. 2.10.c we can see,

$$\frac{\lambda_m - \lambda_{m,min}}{\lambda_{m,min}} = \frac{(1 - p_e)}{EA}\Delta W$$

(2.35)

$$\frac{\lambda_s - \lambda_{s,min}}{\lambda_{s,min}} = \frac{(1 - p_e)(W - \Delta W)}{EA}$$

(2.36)

41

From (2.32) and (2.36), and compared to (2.35)
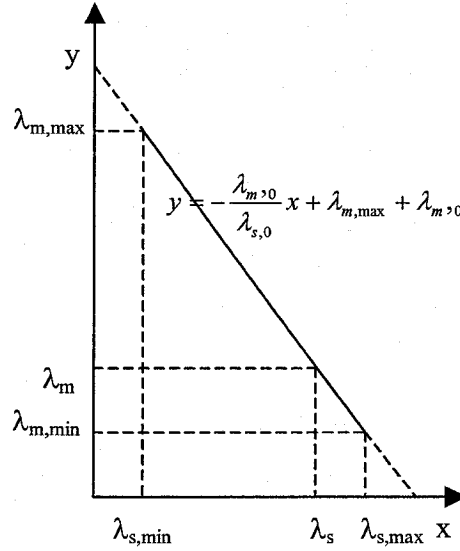
Fig. 2. 11. When the top end of the monitor grating moves down and up, reflected wavelengths, λ_m and λ_s, from sensing and monitor gratings follow the law of a straight line

$$\frac{\lambda_m - \lambda_{m,\min}}{\lambda_{m,\min}} = -\frac{\lambda_s - \lambda_{s,\max}}{\lambda_{s,\min}} \qquad (2.37)$$

Because $\lambda_{s,\min} = \lambda_{s,0}$, $\lambda_{m,\min} = \lambda_{m,0}$ and set $\lambda_m = y$, $\lambda_s = x$, and use (2.33)

$$y = -\frac{\lambda_{m,0}}{\lambda_{s,0}} x + \lambda_{m,\max} + \lambda_{m,0} \qquad (2.38)$$

This straight line is the relation that the reflected wavelength, λ_s, from sensing

grating and the reflected wavelength, λ_m, from monitor grating should obey as the top end

of M grating moves down and up. This straight line has the slope of $-\dfrac{\lambda_{m,0}}{\lambda_{s,0}}$, has the

intercept of $(\lambda_{m,\max} + \lambda_{m,0})$ with Y axis, has the intercept of $(\lambda_{s,\max} + \lambda_{s,0})$ with X axis, and

goes through the two points of $(\lambda_{s,\max}, \lambda_{m,0})$ and $(\lambda_{s,\min}, \lambda_{m,\max})$. This line is as shown in

Fig.2.11. This straight line can called a non-sample line because in the line the load weight

42

W is contributed into the force against D and M grating fibers, or it always keeps $F_m + F_s = W$. It means that S grating fiber and M grating fiber together carry the load weight.

From equation (2.11), assume a starting point is $(\lambda_{s1}, \lambda_{m1})$, and the end point is $(\lambda_{s2}, \lambda_{m2})$, then the wavelength shift is $x = \lambda_{s2} - \lambda_{s1}$, $y = \lambda_{m2} - \lambda_{m1}$. The shift wavelengths follow a simple expressive way

$$y = -\frac{\lambda_{m,0}}{\lambda_{s,0}} x \tag{2.39}$$

2.2.2 Monitor of Load Weight on the Sample

Without a sample, the wavelength shifts follow the law of (2.38) or (2.39). When a sample is located between the range of the displacement of the probe, before probe reaches the sample, the wavelengths shift also follow the law of (2.38) or (2.39), and after probe reaches the sample, the situation has to change.

Two models are proposed and discussed for analyzing the situation that the load and probe contact a surface of a sample. One is an ideal model for the sample without any
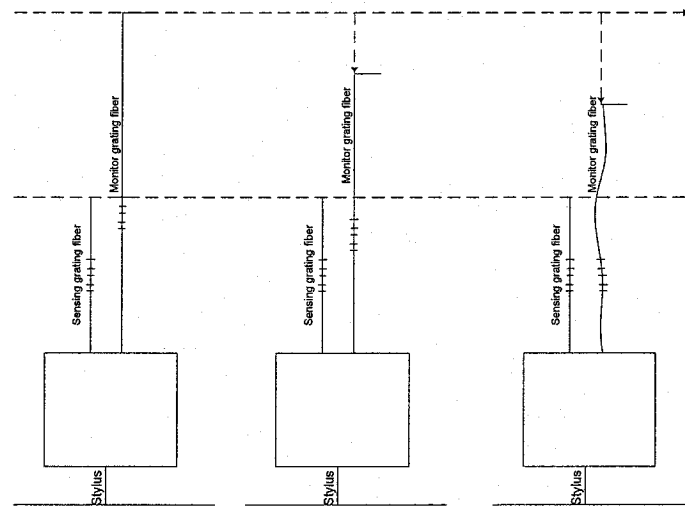
Fig. 2.12. Diagram of an analysis on monitor grating fiber being added.

deformation, and another one considers the deformation.

First we discuss the ideal model. When reaching the surface of the sample, the load and probe is stopped by the sample as shown in Fig.2.12.a. For S grating fiber, when the top end of M grating fiber continues to be down, there is no further reflection wavelength shift from S grating because S grating fiber has no more new elongation if ideally assume the sample and probe are stiff enough to cause no deformation (the ideal model for the sample without any deformation) between the sample and probe in the course from Fig.2.12.a to b and to c. Because S grating fiber does not continue to elongate, the force pulling the grating fiber down keeps unchanged. However, for M grating fiber, it is an elongation decrease procedure when the top end of M grating still continues to be lowered down after the probe reaches the sample. This decrease of elongation will not stop until whole strain of M grating is released as described from Fig. 2.12.a, to b and to c, causing the reflected wavelength from M grating continue to shift from a longer wavelength to a shorter wavelength and the force against monitor grating fiber pulled by the load also continue to become smaller. For the sample, before the load and probe reaches the sample, the sample carries no load weight. After that, the sample begins to stand more and more force come from load. Until M grating fiber is unstrained and the sample obtains the maximum force.

The detail analysis can be made as described in Fig.2.13. For S grating fiber, when and after the load and probe reaches the sample, all values of displacement sensing grating fiber keep in the same due to the sample without any deformation in the ideal model:

$$\lambda_s - \lambda_{s,0} = \lambda_{s,0}(1 - p_e)\frac{l_s - l_{s,0}}{l_{s,0}} \tag{2.40}$$

$$F_s = E \cdot A \cdot (l_s - l_{s,0})/ \, l_{s,0} \tag{2.41}$$

44

$$\lambda_s - \lambda_{s,min} = \lambda_{s,0}(1-p_e)\frac{F_s}{EA} \qquad (2.42)$$

Because $l=l_s$ is fixed, the F_s and λ_s will not change.

a. Without a substrate   b. With a ideal substrate
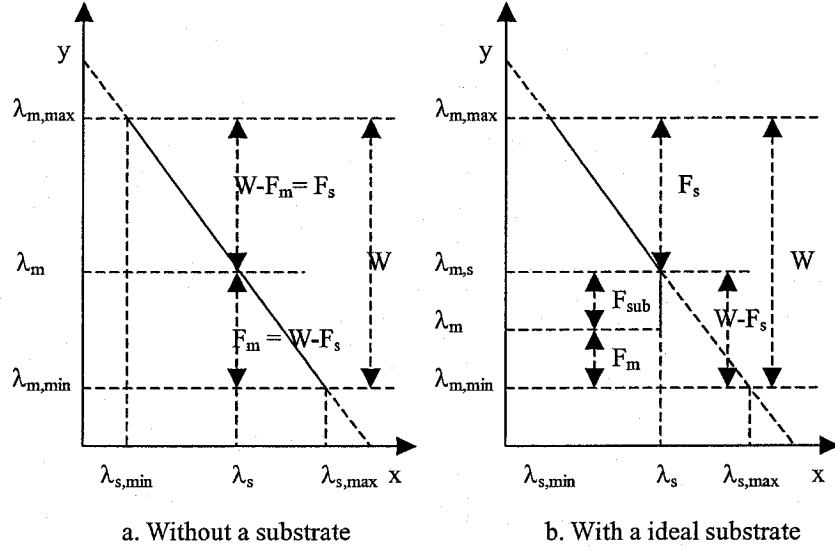
Fig. 2.13. Depiction of forces without and with a substrate

For monitor grating fiber, whatever before and after the probe reaches the sample,

$$\lambda_m - \lambda_{m,max} = \lambda_{m,0}(1-p_e)\frac{l_m - l_{m,max}}{l_{m,0}} \qquad (2.43)$$

$$F_m = E \cdot A \cdot (l_m - l_{m,0})/ l_{m,0} = W - E \cdot A \cdot (l_m - l_{m,max})/ l_{m,0} \qquad (2.44)$$

$$\lambda_m - \lambda_{m,min} = \lambda_{m,0}(1-p_e)\frac{F_m}{EA} \qquad (2.45)$$

$$\lambda_m - \lambda_{m,max} = \lambda_{m,0}(1-p_e)\frac{W - F_m}{EA} \qquad (2.46)$$

When the top end of monitor grating is lowered down, l_m changes, causing the reflected wavelength and the force against M grating to change.

Before the load and probe reaches the sample, $\dfrac{\lambda_m - \lambda_{m,min}}{\lambda_{m,min}} = -\dfrac{\lambda_s - \lambda_{s,max}}{\lambda_{s,min}}$, and has

$F_m = W - F_s$, or $F_s = W - F_m$ as shown in Fig.2.13.a. After the load and probe touches the surface of the sample and the top end of monitor grating fiber still continue to be lowered down, F_m changes smaller and the force against sample, or F_{sub}, appears and become large as shown in Fig.2.13.b. The force against sample can be evaluated by

$$F_{sub} = W - F_s - F_m \qquad (2.47)$$

$$\text{Or } F_{sub} = \frac{EA}{(1 - p_e)} \cdot \left(\frac{\lambda_{m,s} - \lambda_m}{\lambda_{m,0}} \right) \qquad (2.48)$$

where $\lambda_{m,s}$ is the reflected wavelength of M grating when the load and probe just reach the sample. From this equation, it is known that when the probe reaches the sample, $\lambda_m = \lambda_{m,s}$ and the force against sample is 0. After the probe has reached the sample, the force against sample is determined by $(\lambda_m - \lambda_{m,s})$, or determined by other forces, $F_{sub} = W - F_s - F_m$, which is shown as the vertical solid line in Fig. 2.13.b. When M grating fiber is unstrained, $\lambda_m = \lambda_{m,\min}$, and the force against sample is the maximum value of $W - F_s$. Although it is an ideal model with no deformation of the sample, it is helpful for us to understand the real situation that the sample has the deformation after the probe contacts it.

From the above analysis, it is known that M grating which is introduced can be used to monitor the force against the sample by monitor grating's reflected wavelength.

2.2.3 Determination of the Force Against Sample and the Deformation

The model considered the sample deformation after the probe contacts a surface of a sample is discussed here for analyzing the force against sample and the deformation.

When the load and probe reaches the sample,

$$\lambda_{s,sur} - \lambda_{s,0} = \lambda_{s,0}(1 - p_e) \frac{l_{sur} - l_{s,0}}{l_{s,0}} \qquad (2.49)$$

where $\lambda_{s,sur}$ and l_{sur} are the reflected wavelength from S grating and the elongation of S grating fiber when the load and probe reach the surface of the sample, respectively. The point ($\lambda_{s,sur}$, $\lambda_{m,sur}$) is the transit from the non-sample line to the deformation curve, indicating that the probe just reach the surface of the sample at this point.

After the probe has touched the sample and the top end of monitor grating fiber is still lowered down, reflected wavelengths from D and M gratings still change. The deformation forms at the interface between the probe and the sample. The deformation l_d (if deformation just happens to the sample's material and no deformation to the probe material, the l_d is the penetrate depth of the probe into the sample) can be defined by (l_s-$l_{s,sur}$), the difference between the elongations of S grating fiber caused when the probe reaches sample's surface and when the probe has indented into the sample as shown in Fig.2.14.

$$l_d = l_s - l_{s,sur} = \frac{l_{s,0}}{(1-\text{p}_\text{e})} \frac{\lambda_s - \lambda_{s,sur}}{\lambda_{s,0}}$$

(2.50)

The value of $\lambda_{s,sur}$ can be obtained by experiment by approaching (λ_s, λ_m) along the deformation curve towards the non-sample line of $y = -\frac{\lambda_{m,0}}{\lambda_{s,0}} x + \lambda_{m,\max} + \lambda_{m,0}$, or by finding the intersection of the deformation curve and the non-sample line.
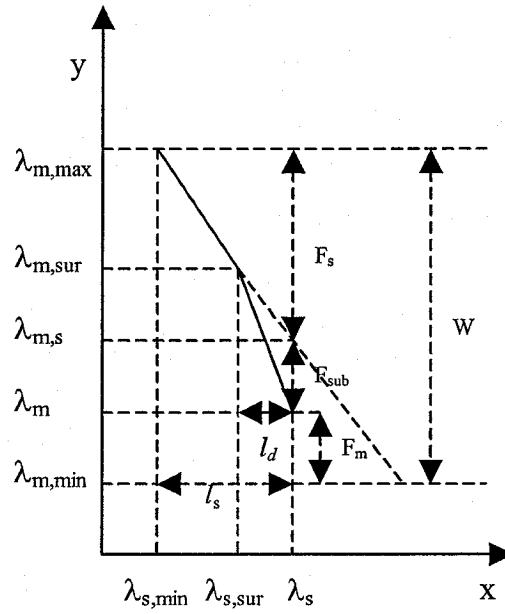
Fig. 2. 14. Depiction of the force against substrate, F_{sub}, and its relation with other forces, and the deformation L_d caused by the interaction between the probe and the substrate

Also from Fig.2.14, the force against sample can be evaluated by

$$F_{sub} = W - F_s - F_m \tag{2.51}$$

$$F_{sub} = \frac{EA}{(1 - p_e)} \cdot \left(\frac{\lambda_{m,s} - \lambda_m}{\lambda_{m,0}} \right) \tag{2.52}$$

where $\lambda_{m,s}$ is the y value in the equation (2.38) obtained by putting λ_s into the equation instead of x. Eq.(2.50) and (2.52) can be used to control and measure the applied force and the material surface deformation.

2.2.4   Control of the Load Weight on the Sample

By M grating fiber and using the relations of

$$F_{sub} = \frac{EA}{(1 - p_e)} \cdot \left(\frac{\lambda_{m,s} - \lambda_m}{\lambda_{m,0}} \right) \tag{2.53}$$

48

we can monitor the force against the sample, and also can control the value of the force.

At first, without a sample, carry out the procedure to determine the non-sample

line $y = -\dfrac{\lambda_{m,0}}{\lambda_{s,0}} x + \lambda_{m,\max} + \lambda_{m,0}$. And then putting a sample within the measurement range,

move the top end of M grating fiber down to allow the load and probe to approach the

sample surface. While approaching, measure the points of λ_m and λ_s, and put λ_s in the

measured non-sample line to determine $\lambda_{m,s}$ and finally put λ_m and

$\lambda_{m,s}$ into $F_{sub} = \dfrac{EA}{(1-p_e)} \cdot \left(\dfrac{\lambda_{m,s} - \lambda_m}{\lambda_{m,0}} \right)$, which determines the force against the sample. Use

an acceptable difference $\lambda_{m,s} - \lambda_m$, such as 0.02nm, or an acceptable amount of F_{sub} as a

control criterion, to control the force against the sample. The control criterion should be

considered over the normal deviation of experiment error from the non-sample line.

2.2.5   Influence of the Deformation on the Step Height Measurement

When we measure a step on a flat surface, first we use the probe to measure the top

surface and then the bottom surface. When the top surface of the step is measured, the

measurement will follow the curve ABC shown in Fig.2.15, A is the beginning contact of

the probe to the top surface of the step, C is in the condition that M grating fiber is

unstrained or the deformation is in maximum value. When we measure the bottom surface

of the step, the measurement will follow the curve DE, D is the beginning contact of the

probe to the bottom surface of the step, E is in the condition that M grating fiber is

unstrained or the deformation is in maximum value. The step height is determined by point

A and point D or by $\lambda_{s,A} - \lambda_{s,D}$. In experiment, we could just draw a short deformation

curve to find the beginning contact point, so using two-grating system can measure the step

height. However, without M grating fiber or M grating fiber is finally unstrained, the step

height is determined by C and E or $\lambda_{s,C} - \lambda_{s,E}$ shown in Fig.2.15. From the diagraph, it is

easy to see $\lambda_{s,A} - \lambda_{s,D} < \lambda_{s,C} - \lambda_{s,E}$. Thus, without control the force on the sample, the step

height result is less than the truth.
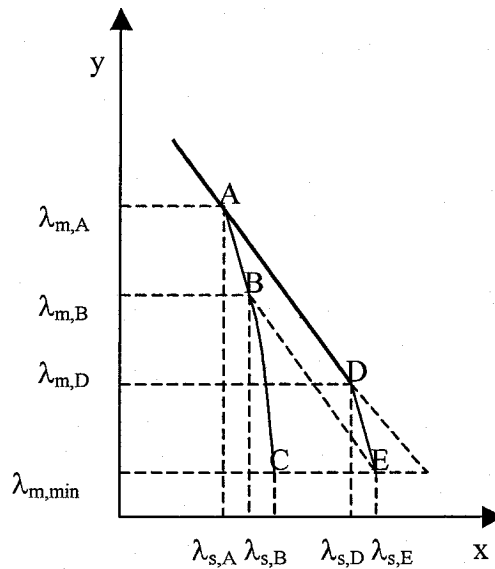
Fig.2.15 Influence of the deformation on the step height measurement

Next we discuss step height measurement with some deformation, which may be

used in automatic measurement instrument. Theoretically, it can be assumed that the

properties of the top and the bottom surface material are the same. Therefore, the curve

ABC has the part, such as curve AB, repeating the curve DE because they cause the same

deformation by applied the same forces F_{sub} (or $F_{subB} = F_{subE}$, or in the condition of

$\lambda_{m,A} - \lambda_{m,B} = \lambda_{m,D} - \lambda_{m,E}$ from M grating fiber) in the same procedure. And the straight

line AD in solid is parallel to the straight line BE in dash. The step height l_{step} can be

calculated depended on point A and D,

$$l_{step} = l_A - l_D = \frac{l_{s,0}}{(1-p_e)} \frac{\lambda_{s,A} - \lambda_{s,D}}{\lambda_{s,0}} \qquad (2.54)$$

Ideally curve AB is the same as curve DE, $l_A - l_D = l_B - l_E$, step height can be measured by

$$l_{step} = l_B - l_E = \frac{l_{s,0}}{(1-p_e)} \frac{\lambda_{s,B} - \lambda_{s,E}}{\lambda_{s,0}} \qquad (2.55)$$

Moreover, the equation (2.55) can apply for the condition when E has not reached to an unstrained point or $\lambda_{m,min} < \lambda_{m,E}$ and when applied forces on the top and the bottom surfaces of a step are the same, or $\lambda_{m,A} - \lambda_{m,B} = \lambda_{m,D} - \lambda_{m,E}$ because at these two relative points, the deformations caused by the probe are the same for the top and the bottom surface of a step. In short, when measuring a step height, if we keep the same applied force (less than or equate to $F_{sub E}$ and $F_{sub E}$ being the maximum) to the surfaces of the top and the bottom of the step or keep $\lambda_{m,A} - \lambda_{m,B} = \lambda_{m,D} - \lambda_{m,E}$ ($\lambda_{m,min} \le \lambda_{m,E}$) by controlling M grating, theoretically the measured the step height can be obtained by equation (2.55). Using M grating to monitor and control the applied force against the sample can result in a good measured step height.

Two grating system provides us a good understanding of sample's deformation with the applied force against the sample, gives a proof that controlling an applied force for surface topography measurement is necessary.

CHAPTER III

PREPARATION AND EXPERIMENTAL SET-UP

This chapter presents works in preparation and experimental set-up. At first, three experiments are made to check the feasibility of FBG application for fine measurement. The preparation experiments using long FBG fiber determines whether or not the work to be continued and make progress in the fine measurement field. Next, the components of the set–up for fine measurement, step preparation and SEM micrography, deformation simulation and stage calibration are described.

3.1 Long FBG Fiber Experiment

3.1.1   Reasons for Using Long FBG

Three different experiments were explained in this chapter for investigation of FBG for different purposes.

(1) The first one is using load and probe. The first experiment is designed to simulate the fine displacement measurement condition except for the sensing length of the FBG fiber. The experiment directly investigates the feasibility of applying FBG on the fine displacement measurement. The result of the experiment shows that the load through a probe can stand on a flat hard surface. This experiment successfully demonstrated the use of the FBG fiber for further fine displacement measurement.

(2) In the second experiment, grating fiber is directly fixed to the vertically moving part of stages. The purpose of the second experiment is to investigate the response of FBG fiber to the displacement.

(3) In the third experiment, weights as load were connected to the measured fiber at the bottom end of a long fiber and were hung in the air. The purpose of this third

experiment is to investigate the response of FBG fiber to the load.

Although the theoretical analysis for the fine displacement measurement was made in Chapter II, the real situation should be checked in experiment. For example, whether or not is the reflected peak stable when the load doesn't move? The experiment through a long FBG fiber is an easy way to check the sensing behavior of FBG because it is easy to handle and obtained a good result. The big elongation of a long fiber can be measured by a gauge with accuracy of 0.01 mm. The accuracy of the measurement could be high with a long FBG fiber (if it is 1000 mm long and has 5mm measurement error, it still has good accuracy of 0.5%). The string of sensing fiber can be easy to keep in vertical with less error because of its long length.

The most important reason of using a long grating fiber is that using the longer FBG fiber can expect the properties of the fine elongation of a FBG fiber used in fine displacement measurement. Expectation of properties for fine measurement can be made by long FBG based on the principle that the reflected wavelength is dependent on the axial strain of the FBG fiber. We write the relation between reflected wavelength and strain again here,

$$\Delta\lambda_B = \lambda_B\,(1\text{-}p_e)\varepsilon \tag{3.1}$$

$$\text{or} \quad \Delta\lambda_B = \lambda_B(1\text{-}p_e)\frac{\Delta l}{l} \tag{3.2}$$

Where $\Delta\lambda_B$ is in nm, l and Δl are the length of the sensing part of FBG fiber and its elongation, respectively. The stain is $\varepsilon = \dfrac{\Delta l}{l}$.

The equation (3.2) indicates that if $\dfrac{\Delta l}{l}$ remain the same, the reflected light from the

Bragg grating will cause the same shift of $\Delta\lambda_B$. The reason is that the same $\dfrac{\Delta l}{l}$ causes the

same elongation for a same Bragg grating section inscribed by UV laser light in the fiber,

or say, causes the same photoelasticity for a same Bragg grating. The explanation for this

concept can be shown in Fig.3.1. The grating fiber b is three times longer than a, and the
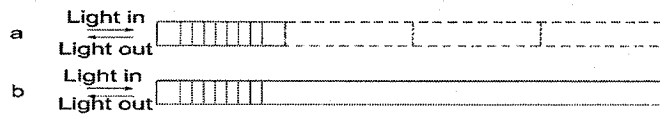
Fig.3.1. The grating fiber b is three times longer than a, and the elongation of
b is also three times longer than that of a. a and b have the same strain, and
the inscribed grating in a or b feels in the same condition, causing reflected
wavelength in the same shift.

elongation of b is also three times longer than that of a. a and b have the same strain, and

the inscribed grating in a or b feels in the same condition, causing reflected wavelength

with the same shift. So if you want to know a short grating fiber's behavior, such as the

relation between elongation of the fiber and the wavelength shift, you can investigate a

long grating fiber's behavior.

3.1.2   Long FBG Fiber Experiment Using Load and Probe

3.1.2.1 Set-up

A schematic of the set-up for measuring the photoelasticity of FBG fiber by using

load and probe is set up as in Fig.3.2. The real set-up is shown in Fig.3.3.

The measurement system consists of a horizontal X-Y coarse stage, a vertical Z

stage (an heavy optical jack), a load and a metal probe, a displacement gauge, an the optical

spectrum analyzer (OSA), a circulator and an optical Bragg grating fiber whose sensing
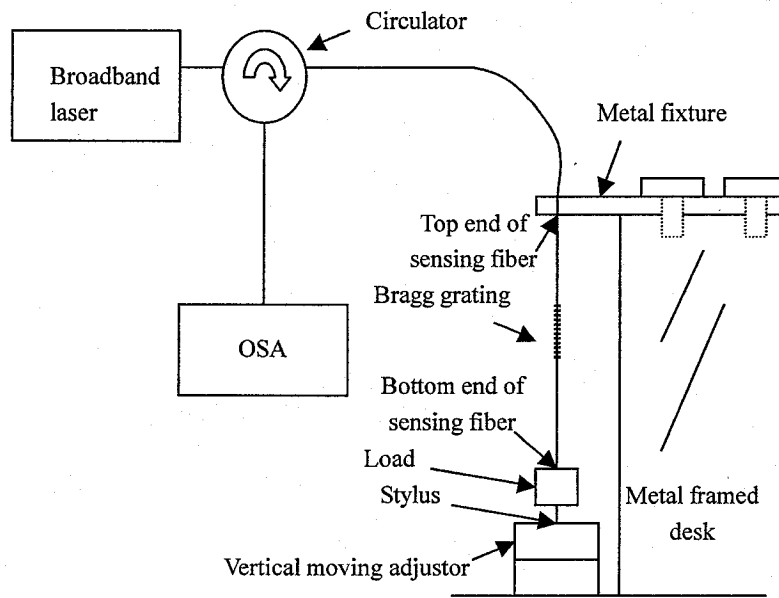
Fig. 3. 2. Schematic of test for photoelasticity of FBG fiber using load and probe

part has a length of 1206 mm.

The top end of the sensing FBG fiber was mounted with glue to a metal fixture
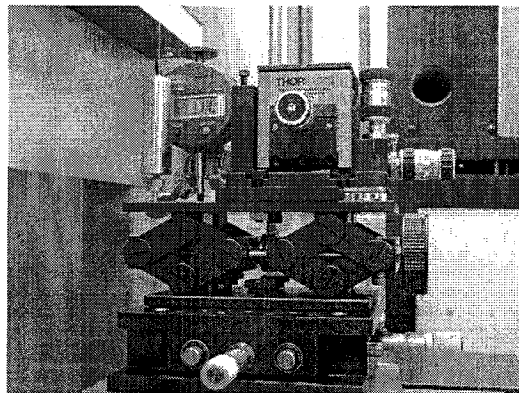
Fig. 3. 3 Measurement set-up for
photoelasticity of FBG fiber using load
and probe.

fixed to a side of a heavy metal-framed lab desk. The bottom end of the sensing fiber was

glued to a 150g steel load. A metal probe is connected to the bottom of the load. The

displacement gauge and probe of a 150g load both touch the top surface of the optical jack, a vertical movement adjustor. This experiment shows when the surface of the jack vertically moves down, the probe and the load are also vertically moving down and cause the fiber to elongate. The expansion value of the sensing fiber can be read on the screen of the displacement gauge.

This first experiment is also designed to test the performance of the load and probe to check whether or not the load through probe can vertically stand on a horizontal surface.

3.1.2.2 Result and Analysis for Experiment Using Load and Probe

The result of the first experiment to measure photoelasticity of FBG fiber using load and probe is shown in Fig.3.4. The value of Y-axis is the reflected wavelength obtained from OSA. The X-axis is displacement of the surface of the jack on which probe touched.

From Fig.3. 4, we can see that:

(1) There is strong linear relationship between the elongation of the sensing part and the shift of the reflected wavelength of grating because the solid straight line in Fig.3.4 is the trend line of the data with regression coefficients $r^2 = 0.9999$. This linear response is the reason that FBG fiber can be used in the displacement measurement as a displacement gauge.

(2) According to Fig.3.4 the linear relationship between the elongation of the fiber and the reflected wavelength shift is equal to $\Delta\lambda_B = 0.9613\Delta l$, where Δl is in mm.

Compared to theoretical value $\Delta\lambda_B = 1200 * \dfrac{1546.8427}{1550} * \dfrac{\Delta l}{1206mm} = 0.9930\Delta l$, the relative error is less than 0.2%.

56

$$y = 0.9613x + 1546.8426$$
$$R^2 = 0.9999$$
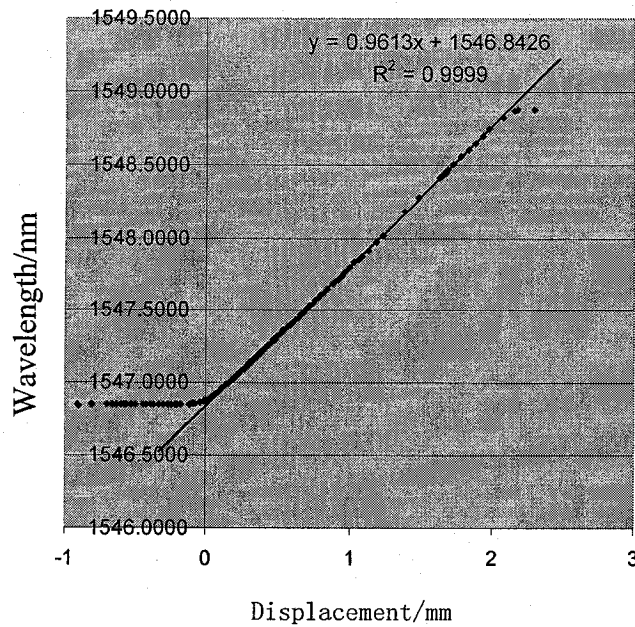
Fig. 3. 4. Reflected wavelength vs displacement
using load and probe

(3) This experiment has assured that the load and probe can stand on a flat surface

when the surface is in stationary or moves from a height to another, keeping FBG

fiber straight and vertical. It confirms the feasibility of using FBG on the fine

measurement.

3.1.3 Photoelasticity of FBG Fiber Versus Length Variation

The second experiment was performed by the load being fixed to the top surface of

the jack by steel metal fixture, resulting in no relative motion between the bottom end of

sensing fiber and the vertical moving surface of the optical jack.

The result of the second experiment for photoelasticity of FBG fiber fixed to vertical

moving part is shown in Fig.3.5.

From Fig.3.5, we can see that:

57

(1)There is a perfect linear relationship between the elongation of the main sensing

part and the shift of the reflected wavelength because of the trend line in Fig.3.5 with
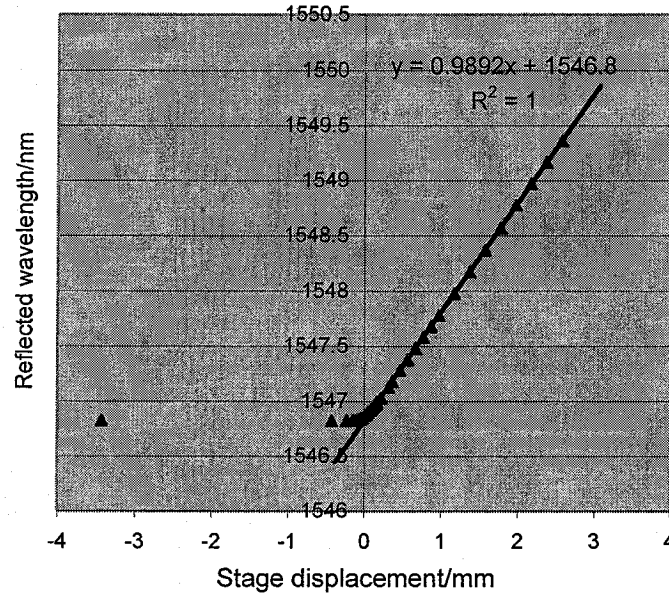
Fig. 3.5 Reflected wavelength vs displacement of the surface of a
vertical moving jack

regression coefficients r^2 =1. This experiment indicates FBG is a perfect linear

displacement sensor.

(2) The linear relationship between the linear elongation of the fiber and the reflected

wavelength shift may be $\Delta\lambda_B = 0.9892\Delta l$, where Δl is in mm. Compared to the theoretical

result, $\Delta\lambda_B = 0.9930\Delta l$, the relative error is less than 0.4%.

(3) Fine displacement measurement resolution can be expected. In Fig.3,6, there were

8 peaks produced when the heights of the top surface of stage changed from 4.92 mm to

4.99 mm with incremental step of 0.01mm determined by a displacement gauge. The FBG

fiber was also elongated in the same steps, causing the reflected wavelength to shift ~0.01

58

nm per 0.01mm movement. Because the resolution of OSA is 0.01 nm shown in one grid
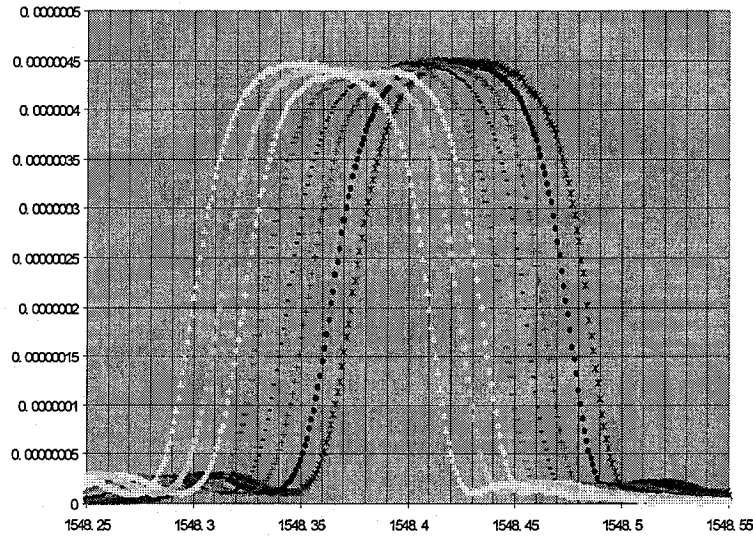
Fig. 3. 6. Reflection peaks produced when positions of the top surface of stage changed from 4. 92 mm to 4. 99 mm with incremental step of 0. 01mm

width in the diagram in Fig.3.6, and a step shift of the wavelength is almost the same as the

resolution value 0.01 nm, we can say that this FBG fiber system can identify a 0.01mm

change of the surface of the stage. For one 0.01mm elongation of the 1206 mm, we can

assume it is contributed by 100 pieces of 0.1 micron elongations from 100 pieces of small

fibers. The length, X, of one small piece of the fiber can be found by

$$1206 \text{ mm} : 0.01\text{mm} = X : 0.1 \text{ } \mu\text{m}.$$

or $\qquad$ X= (1206/0.01)*0.1 = 12060 μm $\approx$ 12 mm.

Based on the experiment, we can expect that a position change of 0.1 micron can be

detected by using a 12 mm long grating fiber, which produces a 0.1 micron fiber elongation

and makes a 0.01nm shift in OSA matching the resolution of the instrument. If the grating

fiber is shorter than 12 mm, the displacement measuring resolution can be improved.

(4) This experiment also gives the evidence that if a FBG fiber is used to measure the displacement in the scale of mm by directly using its elongation effect, the length of the FBG fiber should be as long as 1 meter, which may limit the use of FBG in a macro scale.

Although FBG fiber is hardly and directly used in the macro field, the experiment on photoelasticity of FBG fiber with length as a variable provides an expectation for the FBG fiber that can be used as good sensor for sensing fine displacement and can be used for the displacement measurement due to its linear responsive behaviors.

3.1.4 Long FBG Fiber Experiment with Load as a Variable

The third experiment for the photoelasticity of FBG fiber is performed by top end of sensing part of the FBG fiber being fixed as the same as the first and second experiment
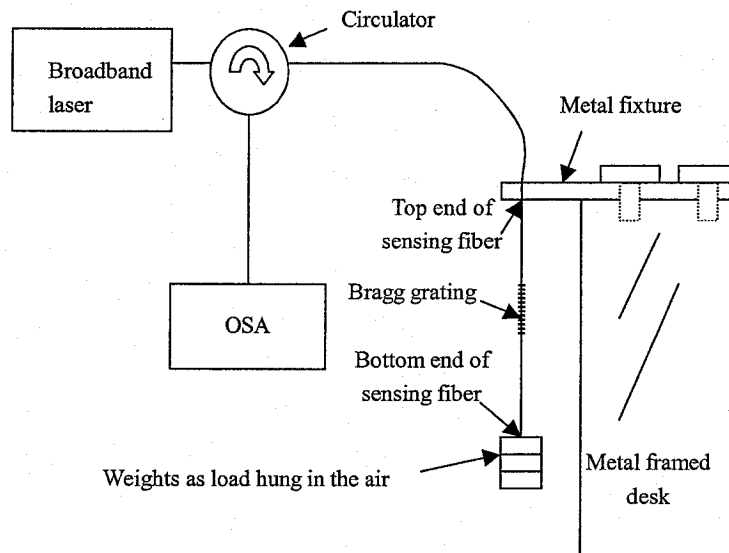
Fig. 3.7. Schematic of test for photoelasticity of FBG fiber loaded by weights

did, but the bottom end of the fiber is glued to 10g holder which is hung in the air. Under test, 19 pieces of standard weights (10g of each) were added piece by piece on the weight holder to increase the load to the sensing fiber. Thus, including no load and the 10g holder,

21 experimental data (from 0 g to 200g in 10g incremental step) were obtained in this
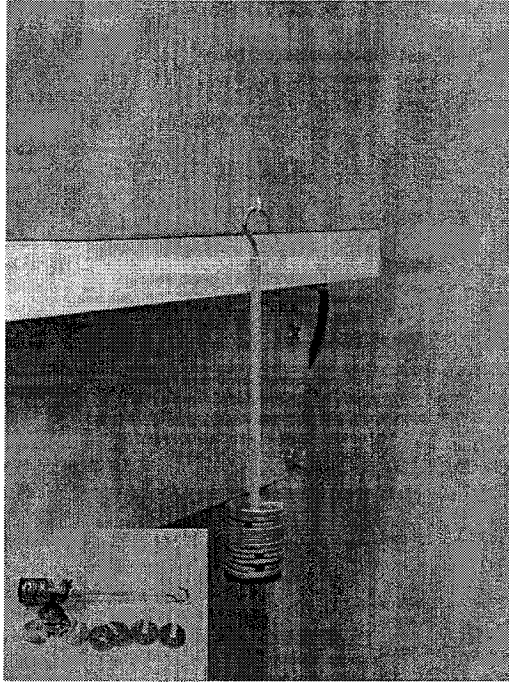
Fig.3.8 Weights as a load directly make a FBG fiber to
elongate

experiment. This experiment as shown in Fig.3.7 is designed to directly investigate the

relation between the shifts of the reflection wavelength $\Delta\lambda_B$ and the load (weights) without

any other distortion. Fig.3.8 shows a real image under the test.

The result of third experiment is shown in Fig.3.9.

Hooke's law gives

$$F = E \cdot A \cdot \varepsilon = E \cdot A \cdot \Delta l/l \qquad (3.3)$$

where F is the force applied to the fiber, E is the elastic modulus, A is the cross sectional

area of the fiber, $\varepsilon = \Delta l/l$ is the strain or longitudinal deformation. From equation (3.2) and

(3.3), we have

$$\Delta \lambda_B = \lambda_B (1 - p_e) \frac{\Delta l}{l} = \lambda_B (1 - p_e) \frac{F}{EA} \qquad (3.4)$$

A is approximately $0.0123 mm^2$. $E=73GPa$. The equation represents the change in the
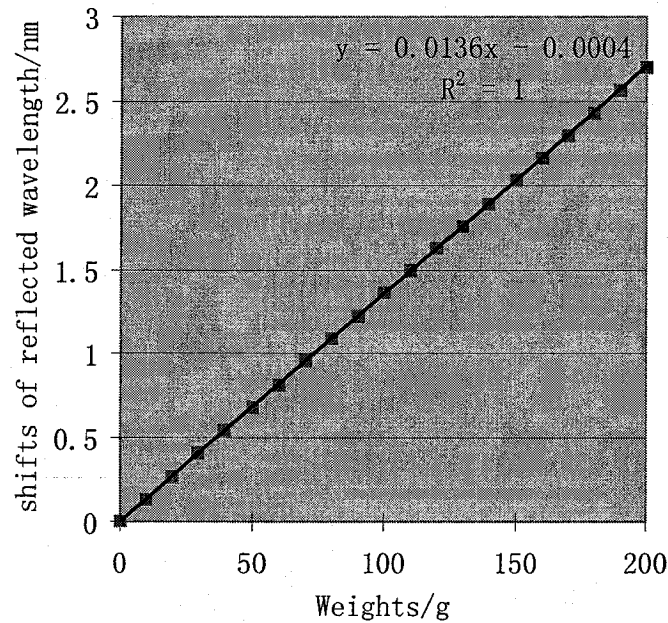
Fig. 3.9 Wavelength reflected from the FBG with respect to
the stretching load

wavelength reflected by the FBG with respect to the stretching force of load or weights.

The Young's modulus of the transducer was used in order to obtain the strain from the

applied force.

For λ_B=1550nm grating fiber, $\Delta \lambda_B = 11.33 \times 10^{-2} F$.

For λ_B=1546.83nm grating fiber $\Delta \lambda_B \approx 1.33 \times 10^{-2} F$

where unit of F is gram or gf.

From the trend line of the experiment data in Fig.3.7, $\Delta \lambda_B = 1.36 \times 10^{-2} F$.

Compared to the theory result, the relative error is 2%. The reason of the

experimental value higher than the theoretical one may be that the 19 weights (10g for

each) and the 10g weight holder chosen were all slightly heavier than 10g.

The weight of load used in the first experiment is 150.199g, causing 2.02nm the

reflected wavelength shift from unstrained condition and resulting in $\Delta\lambda_B = 1.34 \times 10^{-2} F$.

Compared to the theoretical result, the relative error of experiment
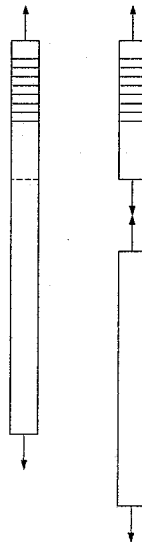
Fig. 3. 10. The same applied force causes the same elongation of a
grating section no mater the length of the FBG fiber.

result will be less than 1%. The conclusion is the experiment matches the theory. In future

work can use the theory to directly evaluate the reflected wavelength shift caused by a load.

The significance of the equation (3.4) is that no mater how long the FBG fiber is,

the reflected wavelength can be known if we know the weight of the load applied to the

fiber. An experiment also has been made by a shorter length of FBG sensing fiber to

confirm that two different lengths of a FBG fiber have the same response to the same

weight. The explanation can be described in Fig.3.10. When the top end A of the sensing

fiber is fixed and the bottom B is loaded. Under the test, this sensing FBG fiber is

stationary, and there is no net force acting on the fiber. The force from load pulling the

fiber downward is equal to the force from the fiber fixing holder, or $F_b = F_a$. This time the

reflected wavelength is $\Delta \lambda_B$. In this condition, in the sensing fiber we analyze an any point, say point C, at which there is a force F_c pulling the higher part downward and a force F_c' drawing the lower part up, and $F_c = F_c' = F_b = F_a$ in stationary. This situation is as the same as following one. If the fiber is cut at point C, and put the same load F_b (as the former condition) to position C (the new bottom end of the remaining higher part), the reflected wavelength from the grating is in the same value of $\Delta \lambda_B$ because the grating section in fiber feels like in the same condition. Therefore, no mater how many the FBG fiber's length and elongation are, if the pulling force(load or weight) is known, the grating's reflection wavelength can know. This concept will be used in monitor grating fiber to monitor and control the force against the sample, whose length is not important and can be chosen in the controlled range of a stage.

The third experiment proves that the theory is right, and the experiment was well done.

The experiment on photoelasticity of FBG fiber with load as a variable provides another understanding of a FBG fiber that it can be used to linearly sense the force against fiber, based on which the applied force against the sample can also be sensed.

3.1.5 Conclusion for Long Grating Fiber Measurement

Experiments on long FBG fiber is used to confirm the feasibility of using FBG for the fine measurement for displacement sensing and force sensing.

The experiment with long FBG fiber using load and probe simulates the fine displacement measurement condition and demonstrates the use of the FBG fiber for further fine displacement measurement.

The second and the third experiment are designed to separately investigate both

responses of the FBG fiber for the displacement and the load force. The experiment on photoelasticity of FBG fiber with length as a variable provides an expectation for the FBG fiber that can be used as good sensor for sensing the fine displacement and can be used for the displacement measurement due to its linear responsive behaviors. The experiment on photoelasticity of FBG fiber with load as a variable provides another understanding of a FBG fiber that it can be used to linearly sense the force against fiber, based on which the applied force against the sample can be sensed.

Theoretically in Chapter II and experimentally in Chapter IV, the one grating measurement system is a successful application based on using one grating to be able to sense displacement and force against the sample.
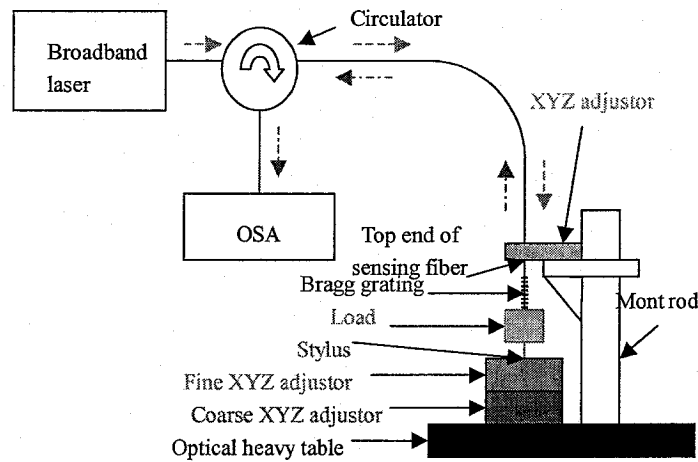
Fig. 3. 11. Schematic of the fine measurement using two grating fibers
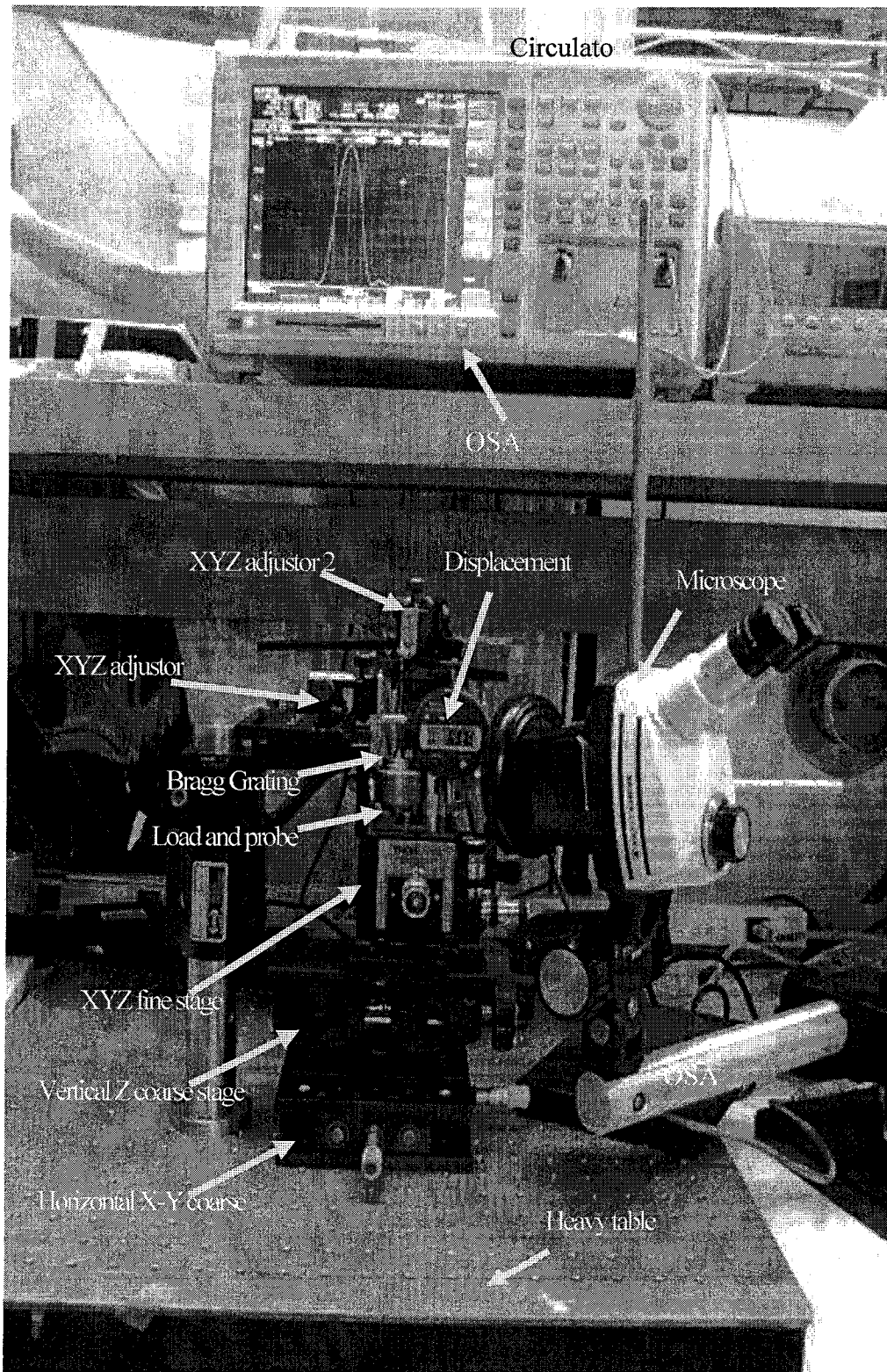
Fig.3.12 Set-up for fine measurement using FBG

Theoretically in Chapter II and experimentally in Chapter IV, the two grating measurement system is a successful application because a grating fiber can sense the displacement and the other monitor grating fiber can monitor and control the applied force against the sample independently.

3.2 Measurement System Set-up for fine measurement

A schematic of the fine measurement is shown in Fig.3.11.The real set-up for fine measurement is established as shown in Fig.3.12. The measurement system consists of an optical heavy table, a horizontal X-Y coarse stage, a vertical Z stage, a horizontal XYZ fine stage, a load, a probe, an optical Bragg grating fiber, two small XYZ adjustors, a microscope, an OSA and a circulator.

Probe: The best material to make the probe is diamond because it is the hardest material in
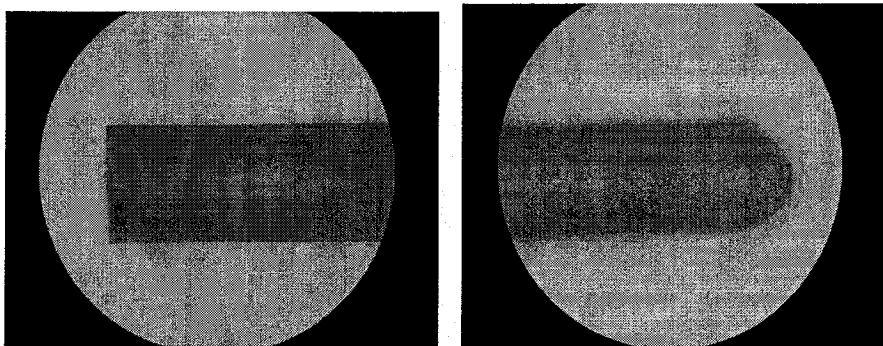
Fig. 3. 13. A tip of a probe is in half sphere in right picture and another end of the probe is in a plane designed to stick into steel metal

the world. There are commercially available probe but they are very expensive and it costs 1200 USA dollars for a diamond probe with the tip in 5μm diameter. Two kinds of probes were made. The first one is made by material of steel. The second is made by ruby. Ruby, like sapphire, is part of the corundum family of minerals that are second only to diamond in hardness. A small ruby bar of $\phi1.44$ mm was ground manually by the writer and shaped

into one end in the shape of half sphere and another end in a plane. The two ends of the ruby probe are shown in Fig.3.13.

Load: loads was designed and made as shown in Fig.3.14. The first load is used for studying the photoelastic behavior of FBG fiber in length of 1206 mm. The second load is used for fine measurement. The main body of the load 2 is made of copper due to its higher density than steel.

The displacement measurement range is determined by the load. The applied strain

a) The first load   b)The Second load
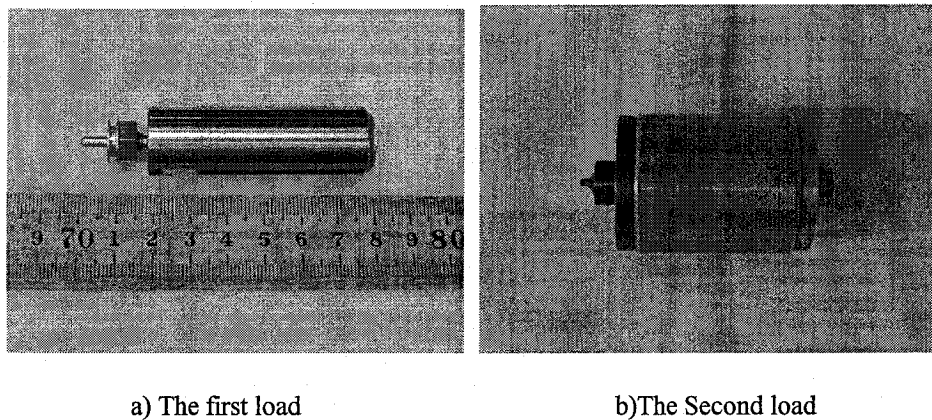
Fig.3.14. Loads used for experiment

to the FBG fiber can be more than $5000\mu\varepsilon$ (500g load) [22], which is enough for the fine displacement measurement, so the possible maximum displacement measurement is not the interest of the thesis. In the long FBG experiment in this chapter applied load of 200g makes the grating work well. The range within $10\mu m$ is sufficient for most surface application. Therefore, a 150g load is designed to use in the material surface measurement.

Optical heavy table: The function of the optical table is to provide a vibration-free environment on its surface for the table mounts.
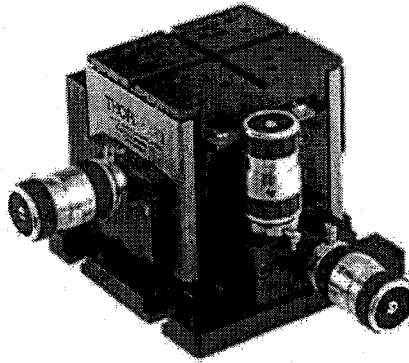
Fig.3.15. MDT616, a 3-axis translation stage

XYZ adjustors: Four XYZ direction control systems are used in my study. Two systems are used for controlling the substrate movement, and the others are two small XYZ adjustors for the positions determination of the top end of displacement and monitor grating fibers.

To control the movement of the surface on which a measured sample or sensing probe can stand, a coarse adjustor system and a fine adjustor system are used. In the coarse XYZ system, two translation stages are for X and Y direction and an optical jack for vertical movement. The coarse XYZ system provides large range movement, whereas the fine XYZ system does the fine adjustment. The fine XYZ adjusting system is 3-axis translation stages shown in Fig. Fig.3.15 called XYZ flexure stages, whose model is MDT 616 made by Thorlabs Inc. The smooth and stable fine motion provided by MDT 616 makes it suited for micropositioning application. Its flexure design yields three orthogonal translation degrees of freedom without the severe limitations of stiction and friction that is found in traditional bearing based stages. Its 200-300μm fine adjustment range covers my study range. One division of 1~ 2 micron, making it can be used for calibrating my sensing system. This fine XYZ system was calibrated by a displacement gauge, reported in this end

of the chapter.

To control the grating fiber and the load as well as control the probe, two small

XYZ adjustors as shown in Fig.3.16 are used. One of both is connected to the end of a
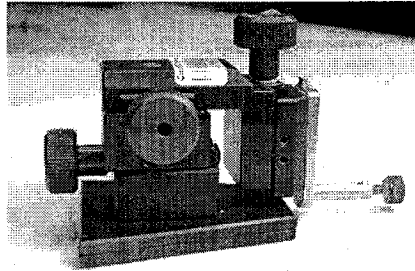
Fig. 3. 16. a small 3-axis stage

displacement sensing FBG fiber and another is connected to the end of force monitor

grating fiber used to drive the load to move up and town and monitor and control the force

against the sample.

Microscope: the microscope used here is to view the position of the substrate touched by

the probe. The microscope can used to choose a region to measure. In Fig.3.17, the
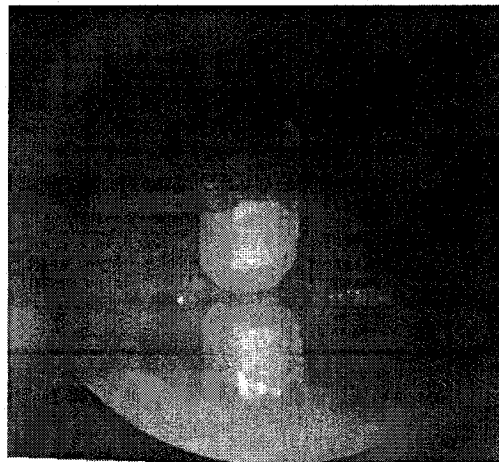
Fig. 3. 17. Microscope can observe the probe and
sample

surface of silicon substrate and also a ruby probe with its reflected image on the surface can be observed through the microscope.

Optical fiber Transmission Window: Among the three matured windows around at 800 nm and 1310 nm and 1550 nm, the 1550 nm system of the longest wavelength technology was used to obtain the highest sensing sensitivity for displacement and the force.

Optical Spectrum Analyzer (OSA): It can display the spectrum of reflected light from the sensing grating. It can show the reflected waveform on the OSA screen and calculate wavelength central position and other parameters of a peak. OSA used for the thesis is a product of Ando Electric. Model is AQ6319, one of the best OSA recently in the world, which provides high accuracy wavelength measurement with the resolution as high as 0.01 nm within the range of 1520-1580 nm. This important factor makes it possible to use FBG to provide fine displacement measurement as the resolution as submicron level.

Optical Fiber and Bragg Grating: In whole of experiments for the thesis, all optical fibers involved in grating production were Corning® SMF-28TM fiber, and all FBG gratings employed in the experiment were inscribed at Bragg Photonics Inc. To meet the high sensitivity requirement, unstrained λ_B of a grating should be as big as possible, and should also keep OSA at the highest resolution of 0.01 nm, λ_B may be chosen at 1575 nm because OSA has the highest resolution within 1520-1580 nm. To meet the high sensitivity requirement, on the one hand l_0 should be as small as possible, on the other hand the recent grating fabrication technology should be considered. In the grating fabrication company, the shortest length of a Bragg grating fiber with the reflection coefficient of 60% can be made as long as just 5.5 mm. Choosing the unstrained characteristic wavelength close to 1580 nm is important for both displacement sensing and force sensing purpose to obtain a

71

good displacement and force sensitivity and resolution of the measurement

Leveler: A leveler was successfully manually made by the writer by using a glass tube and put alcohol in it (the diameter of glass tube doesn't be too small, and ID water failed to fabricate it!). Leveling the top surface of the stages is important for all topography
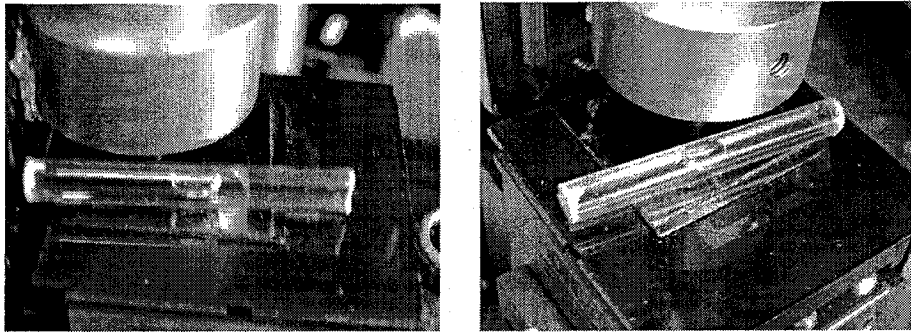
Fig. 3. 18. Hand-made leveler keeps the top surface at a horizontal level

measurements. Even for indentation, leveling is also important, otherwise, the actual contact area between indenter and material is not known from a given indentation depth[53]. Although we used the leveler to confirm the level of the top surface of the stages, the sample surface still made an angle of 0.3° with horizontal plane (see Chapter IV). Fig.3.18 shows the hand-made leveler to keep the top surface plane at a horizontal level by putting the leveler on the surface in two orthogonal directions and adjusting the
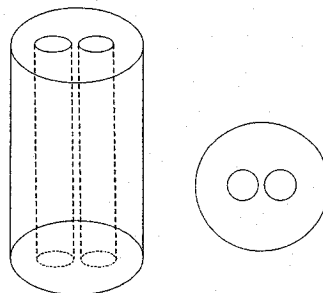
Fig. 3. 19. The shape of the grating fiber holder connected to a small xyz adjustor.
A) is the whole shape of the holder; b) is the cross-section of the holder

72

surface to place the bulb in the middle of the leveler.

Grating Fiber Holder: A holder for grating fiber was designed as shown in Fig.3.19. There are two holes in it. One hole is for fixing the top of the displacement-sensing-grating fiber by glue and another is for a fiber or a force-monitor grating fiber to go through in order to raise up or lower down the load.

3.3 Step Preparation and SEM Micrography

In order to measure the step height by the fine measurement system, some step samples were prepared on silicon wafer surface by etching in 25wt% TMAH solution.

Silicon Wafer: The orientation of Si is {001}. The silicon wafer sample is chosen because it has good flat and smooth surface. Another reason is the wafer sample can be fabricated into a good step sample, whose two step surfaces are parallel to each other.

Mask: To make a step on the silicon wafer, a half transparent and half opaque mask was made.

TMAH Solution: 25wt% concentration of TMAH solution was used in the experiment for making step samples. The most important reason to choose the TMAH to fabricate step samples is that its anisotropic etching produces is suitable for achieving smooth, flat and parallel two surfaces for a step, those features is not able to be created by the isotropic wet etching. The TMAH solution etching shaping silicon by anisotropic etching is constrained by the fact that {111} family of planes confine the etching advancement since the etch rate of {111} planes is much lower than that of any other plane, and can be fairly considered as comparatively equal to zero as the research of Tabata et al demonstrated that the etching rate of {111} plane in TMAH solution is about 0.02-0.05 times smaller than that of {100} plane[54]. The goal of a step sample fabrication is to obtain a 0.1- 10μm step on a silicon

wafer. Because step is not deep, the dry etching techniques such as deep reactive ion etching are not chosen for this processing. The wet TMAH etching using only a temperature controlled bath is chosen for step fabrication also due to its low process cost and high selectivity of masking material of SiO_2. The SiO_2 film can be produced on silicon wafer by oxidation processing in our lab.

Mask of SiO_2 film: The masking film of SiO_2 was produced on silicon wafer in furnace of
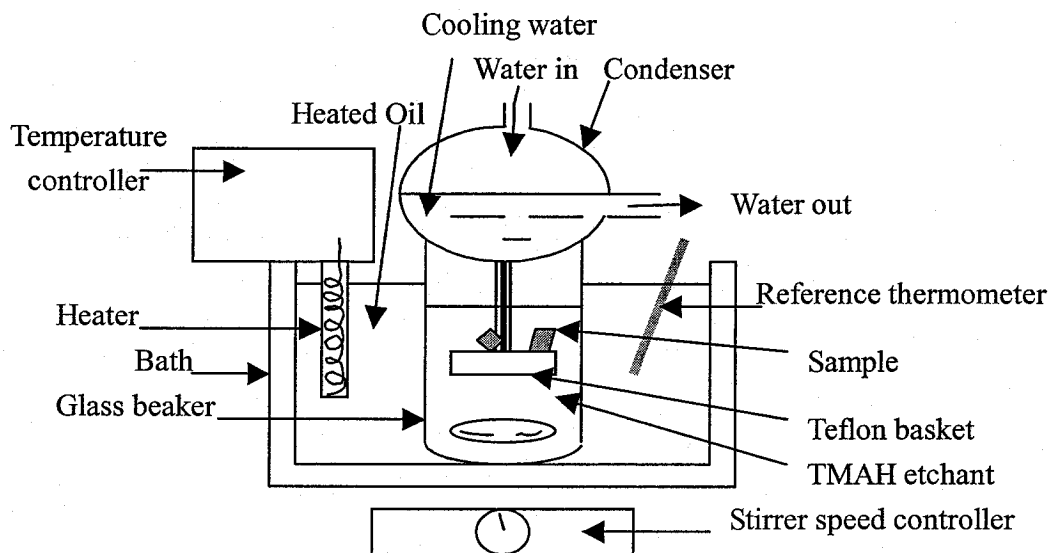
Fig3.20. Set-up of TMAH experiment

$1100°c$ by oxidation processing with of 20 min. The Silicon oxide was etched in the 39%HF. The positive photoresist is used as masking film for SiO_2.

Step Height Determination: Step height is determined by temperature and time. TMAH etching were controlled by temperature through time, not by the concentration of the solution.

Bath and Set-up: A bath is used for TMAH etching. The set-up of the experiment is shown in Fig.3.20. Samples were hold in a Teflon basket and were immersed in the TMAH solution contained in a glass beaker. The temperature of oil in the bath was controlled

within accuracy of ±0.1°C. A thermometer offered a temperature reference. A cooling

water condenser was used so that the etchant vapor can continuously condense for
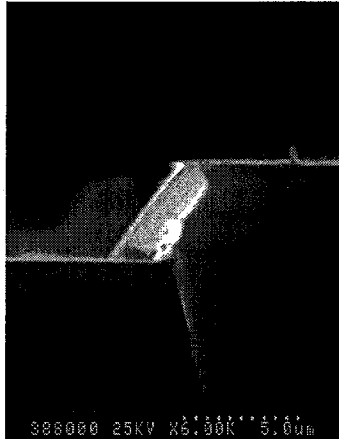
Fig. 3. 21. 12min 90°c TMAH etched step height of 4.3 μm

remaining the TMAH concentration unchanged. The condenser also made the beaker

unmovable. A spinning magnetic stirrer kept the temperature and the concentration of the

TMAH solution in uniform.

SEM Micrograph: Three temperatures were tried for the step etching manufacture.

Fig. 3. 22. 60min 30°c TMAH etched step height of 0.8 μm

The result of step samples was measured by SEM. The SEM adjustment and operation and

75

specimen preparation for SEM observation were done by the author. SEM was adjusted at high resolution (good image in the 20,000× magnification!) and can observe the step in the scale of sub-micrometer. Specimens for SEM were made by dicing in an across section way. At First, 90°c was used. 12 min the step has the height of 4.3 μm as shown in Fig. 3.21. At 90°c the etching time is too short to control, so it is not suitable to control the etching process for step making, then the temperature of 75°c and 30°c were tried. At temperature of 30°c in Fig.3.22, the step of silicon in 60min only has the height of 0.8 μm. Fig.3.22 was in the 15,000× magnification. To get sub-micrometer step, it is better to use the temperature as low as 30°c because it is easy to control the small step height by time.

3.4 Deformation modeling and Simulation

The estimation of the deformation of the surface of the silicon material caused by the probe with an applied force was made by the finite element method (FEM) in the software environment of ANSYS. In this chapter, only preparation of the simulation is presented. The result and discussion is presented in Chapter IV.

The first step is modeling. The finite element model used for this simulation is shown in Fig.3.23, where the silicon substrate is modeled as a cylinder with a radius of 2000μm and a thickness of 500μm. The real size of the substrate is not important for this simulation because the contact region is very small and using a big substrate just results in a long simulation time without any improvement in the results. The half sphere shown in Fig. 3.23 is used to model the ruby and its radius is 720μm. The contact area between the ruby and substrate is just a single point at the beginning and for this reason during the meshing we will use a contact element in FEM as will be explained later.
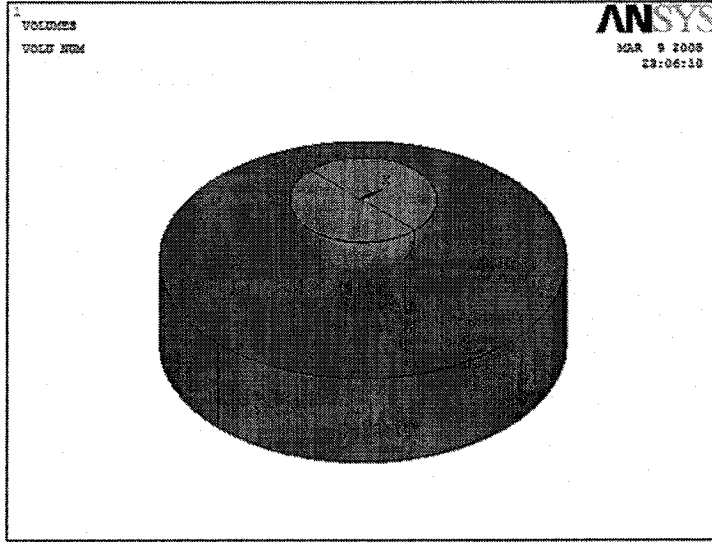
Fig. 3. 23. Schematic of the FEM model used for the simulation

The next step during modeling is to define the material properties. Table 3.1 and

Table 3.2 present the mechanical material properties, Young's modulus, Poisson's ratio,

and density, for the silicon and ruby respectively. As the dimension of the structure is in

micrometers, for the material properties we have also used the μMKS system of units. In

Table 3.1 and Table 3.2, material properties are shown in both systems of units.

Table 3.1 Mechanical material properties of silicon

Mechanical Parameter	MKS System of Units	μMKS System of Units
Young's Modulus	$150 \times 10^9 Pa$	$150 \times 10^3 MPa$
Poisson's Ratio	0.17	0.17
Density	$2330 Kg / m^3$	$2330 \times 10^{-18} Kg / \mu m^3$

Table 3.2 Mechanical material properties of ruby

Mechanical Parameter	MKS System of Units	μMKS System of Units
Young's Modulus	$345 \times 10^9 Pa$	$345 \times 10^3 MPa$
Poisson's Ratio	0.30	0.30
Density	$3980 Kg / m^3$	$3980 \times 10^{-18} Kg / \mu m^3$

After preparing the model, the step is to mesh the structure. This part of simulation

is very challenging due to the extremely small contact area between the ruby and silicon

77

substrate. In order to get an acceptable result the element size near the contact region should be very small. Fig.3.24 demonstrates the mesh which has been used during the simulation. For both ruby and silicon substrate we have used the 3-D, 8-Node, Structural, SOLID185 element. SOLID185 is defined by 8 nodes having three degrees of freedom at each node (translations in the nodal x, y, and z directions). The element has plasticity, hyperelasticity, and large deflection and strain capabilities. It also has mixed formulation capability for simulating deformations of nearly incompressible elastoplastic materials, and fully incompressible hyperelastic materials.

a   b
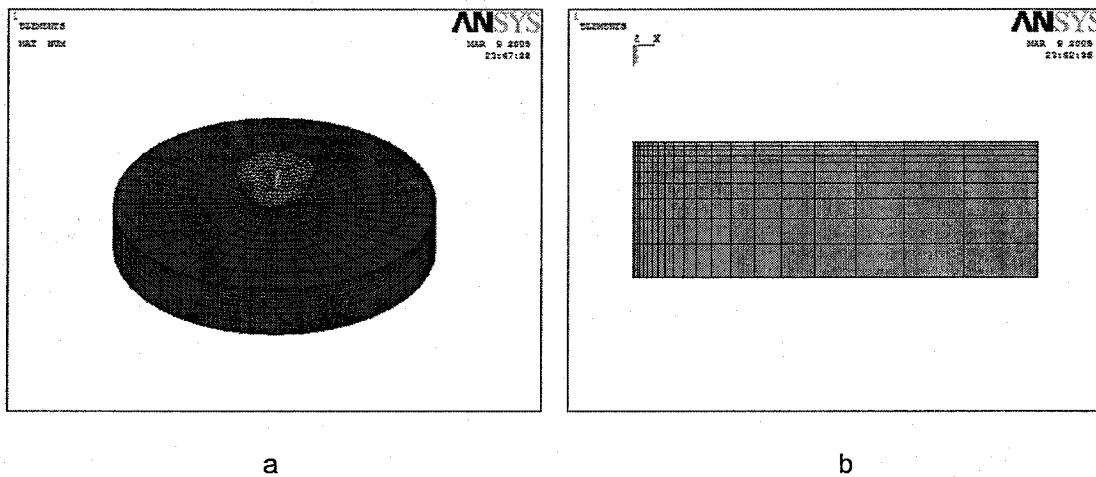
Fig.3.24. (a)Element plot of the mesh for the structures and (b)the for the substrate cross-section

After the structure is meshed with SOLID185 elements then another element is used to define the contact between the ruby and silicon. In contact problems, one needs to identify the surfaces that are expected to come into contact, and group them into either "contact" surfaces or "target" surfaces. There are various approaches for defining contact and target surfaces. One of them is size. If one surface is larger than the other surface, the larger surface should be the target surface. For our problem, the initial interaction between the ruby and substrate is at a point. However, we expect the surfaces of the bodies to come

into contact once the force is applied. CONTA175 is one of the node-to-surface contact elements that can be used to represent contact between a node and a surface or between two surfaces. This element also supports 3-D structural contact analysis and we'll use it to mesh the contact surface. For the target surface, we can use either TARGE169 or TARGE170 elements. Since TARGE169 elements support 2-D analysis and TARGE170 support 3-D analysis, we use TARGE170 elements to mesh the target surface (top plate of the substrate). Contact occurs when the element surface penetrates one of the target segment elements TARGE170 on a specified target surface. As the boundary conditions, the base of the substrate is fixed in all directions and a constant pressure is applied on top of the ruby material. The reason of using pressure is that a force can be uniformly distributed on the top of the ruby.

3.5 Stage Calibration

The one purpose of the thesis is to make a sensing system to measure the fine displacement. In order to know the exact accuracy of the measurement sensing device, it needs to be verified against a reliable and operative calibration. A step height of specimen will be measured by a value of reflected wavelength shift. We should use a calibrated standard value to find the relation of reflected shift to the value of displacement.

For a specific displacement sensing system it is necessary to establish ways to valuate the sensing system. Three ways here are used to be as methods as standard or calibration. One is using a displacement gauge to scale the measuring system. Another is using a step samples. A step sample checked by SEM can be used to check the fine measurement system. The third is scaling a translation stage as a calibrated displacement actuator.

For reliability, a precision XYZ translation stage MDT616 in Fig.3.25 is used.
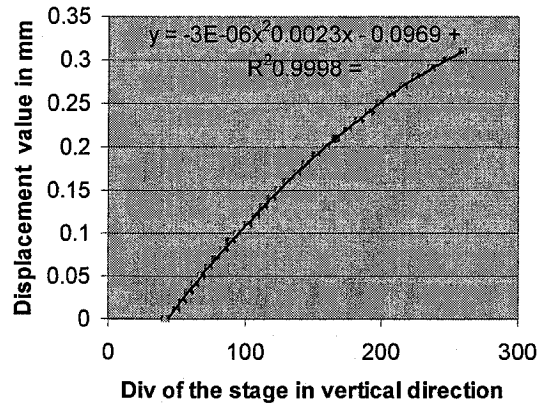
Fig. 3. 25. The stage was scaled by a displacement guage

When it was used to be a stage on which a measured substrate was put, it was found that it was not so precise in its translation movement. So the stage is calibrated by a displacement gauge. The gauge' moving step was 0.01 mm. This stage moving downward and upward was measured by three times presented in Fig.3.25. From the solid trend curve, we can know the scale of the stage is not in a good linear.

CHAPTER IV

EXPERIMENTAL RESULTS

Using the displacement and force sensing properties, FBG fiber can be used to characterize material surfaces. Theories about indentation measurements by using one grating and two gratings are derived in Chapter II. However, those related experiments of two indentation measurements are reported in this chapter. The experiment of measuring the step height is also reported, and experiments are done to check the validity of the theory presented in Chapter II.

4.1 One-grating Indentation Measurement

The one-grating indentation measurement was discussed analytically in section of 2.1.11 in Chapter II. In the experiment, a {100} commercial silicon wafer was investigated by this one-grating indentation measurement. The top end of the FBG fiber is fixed. Heights of the sample were provided by an XYZ flexure stages, which makes the relative movement between the top end of the FBG fiber and the sample. The incremental movement of the sample was made by one division of the vertical axis translation. The values of divisions were calibrated by a displacement gauge reported in Chapter III. When the sample moved up, the probe approached the sample, touched and penetrated into the sample. This was a process to continually raise the force through probe against the sample from 0 to a maximum value to a preset vertical displacement of the sample. In this upward process or loading process, we recorded the reflected wavelength from the grating and the displacement of sample. After that, the sample moved down. This was a process to continually reduce the force against the sample. In this downward process or unloading process, we recorded the reflected wavelength from the grating and the displacement of the

81

sample. Fig.4.1 shows the data of the measured values of the sample vertical displacement h_{dis} versus the reflected wavelength λ from the grating.
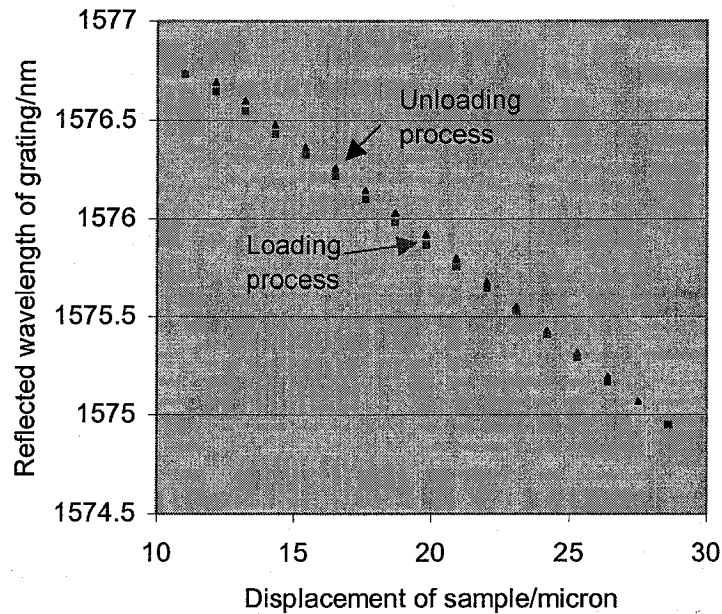
Fig. 4. 1 Experimental result data of a sample displacement related to the reflected wavelength

From the Eqs.(2.29) and (2.30) in Chapter II, we can obtain values of the applied force and the penetration depth. The load-depth curve is drawn in Fig4.2. In this graph, it is clear that the loading curve and the unloading curve can be identified. The difference between loading curve and the unloading curve show that there is some plastic deformation in the loading process although it is small.

The experiment shows that the Bragg grating can be used as an indentation measurement. It is a simple way to measure the load-depth curves as an indentation measurand because a grating can sense both the force and the displacement.

4.2 Two-grating Fibers System

The experiments involved two grating fibers, a displacement-sensing grating fiber
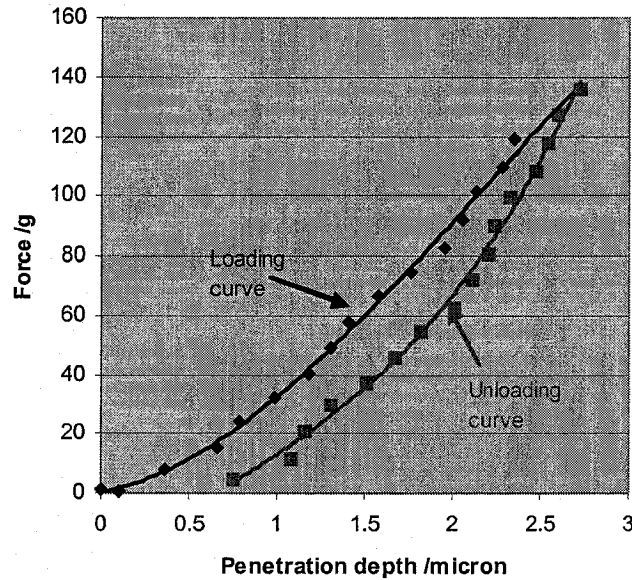
Fig. 4. 2. Indented load-depth curve on silicon wafer using one grating fiber

and a force-monitoring grating fiber, are presented here. Experiments in this chapter are used to check the validity of the theory presented in Chapter II. In these experiments the probe was made of ruby, whose tip is in sphere shape with 1.44 mm in diameter, and the sample is silicon wafer with {001} orientation.

4.2.1 Experiment without Sample and with Sample

In this experiment, at first the probe goes to highest position of its displacement measurement range at which the displacement-sensing grating (S grating fiber) was in unstrained status. As the top end of force monitor grating fiber (M grating fiber) moved down, reflected wavelengths, λ_m from the S grating and λ_s from M grating, were measured by OSA. The experimental data of the reflected wavelengths, λ_m and λ_s, from the

displacement-sensing grating and the force-monitoring grating line is expected in the equation of (2.38) in Chapter II. The comparison between experimental and the theoretical
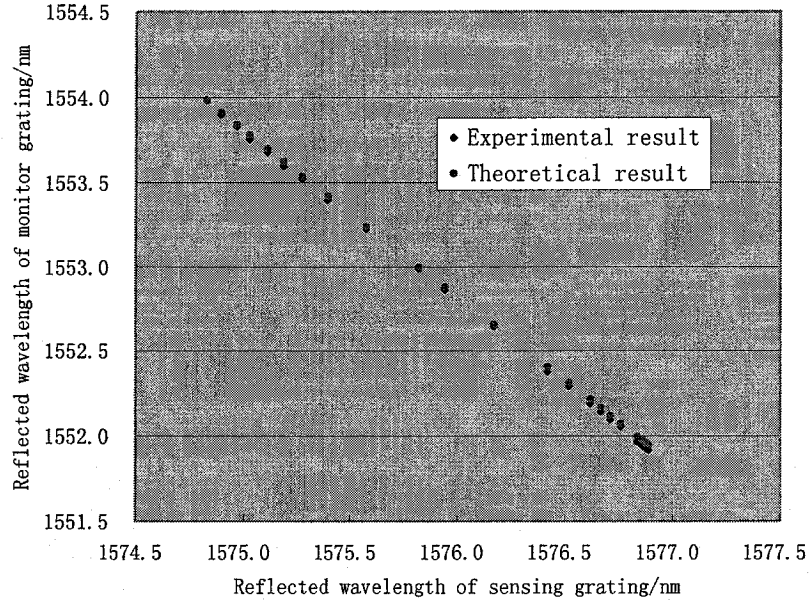
Fig. 4. 3. Comparison between experimental and the theoretical result

result is shown in Fig.4.3.

The theoretical curve of the equation (2.38) is $y = -\dfrac{\lambda_{m,0}}{\lambda_{s,0}} x + \lambda_{m,\max} + \lambda_{m,0}$ .From

two grating parameters, $\lambda_{m,0}$ = 1551.9170 nm, $\lambda_{s,0}$ = 1553.9870 nm and $\lambda_{m,max}$ =

1553.9870 nm, the scope of the line can be calculated as $\dfrac{\lambda_{m,0}}{\lambda_{s,0}} = 0.9855$, and the intercept

of the line with Y axis as $\lambda_{m,\max} + \lambda_{m,0} = 3105.90$ nm. Thus the theoretical non-sample

line could be y = -0.9855x + 3105.9.

The experiment line is obtained by drawing the trend line of the experimental data, that is y = -0.9933x + 3118.2. The slope relative error compared to theoretical result is less than 0.8%. The intercept of the experiment line with Y axis is 3118.2, and the analytical

value is equal to 3105.90, whose relative error is less than 0.4%. The intercept of the experiment line with X axis from the experimental data trend line is 3139.23, whereas the theoretical value is 3151.71, and relative error is <0.4%. The relations between $\lambda_{s,max}$, $\lambda_{s,min}$, $\lambda_{m,max}$ and $\lambda_{m,min}$ in the equation (2.33) and equation (2.34) are capable of being maintained by checking $\dfrac{\lambda_{s,max}}{\lambda_{s,min}} = 1.00131$, $\dfrac{\lambda_{m,max}}{\lambda_{m,min}} = 1.00133$,

and $\dfrac{\lambda_{m,min}}{\lambda_{s,min}} = 0.98545$, $\dfrac{\lambda_{m,max}}{\lambda_{s,max}} = 0.98547$, so $\dfrac{\lambda_{m,max}}{\lambda_{m,min}} = \dfrac{\lambda_{s,max}}{\lambda_{s,min}}$, $\dfrac{\lambda_{m,min}}{\lambda_{s,min}} = \dfrac{\lambda_{m,max}}{\lambda_{s,max}}$.

Another experimental example using different gratings is shown in Fig.4.4. From two grating parameters, $\lambda_{m,0}$, $\lambda_{s,0}$ and $\lambda_{m,max}$, the theoretical non-sample line of the equation (2.38) is y = -1.00104x + 3104.8. The experimental non-sample line is obtained by drawing the trend line of the data, that is y = -1.0159x + 3127.8. From Fig.4.4 and the calculation, it
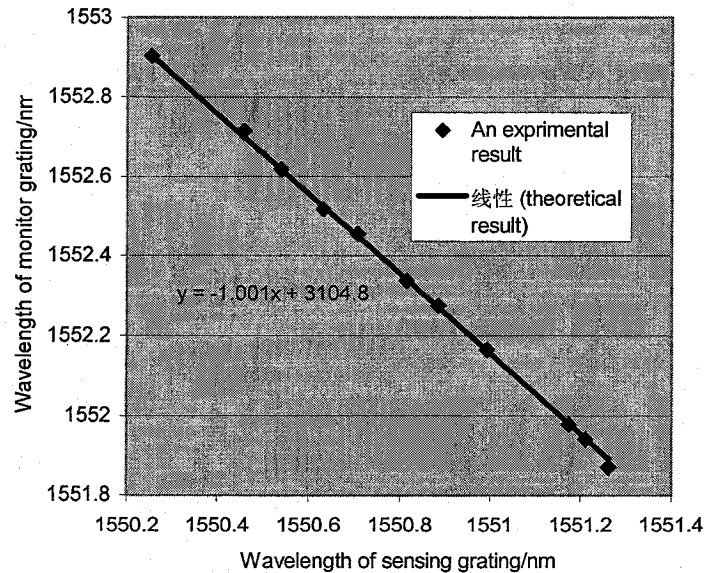
Fig. 4. 4. Another experimental example of reflected wavelength of the sensing grating vs that of M grating and its comparison with the theoretical result

85

is shown that the experimental result matches the theoretical result.

Without a sample, the load and probe can move down and up in the whole range, and the experiment result follows the theoretical law as described by equation (2.38) and as shown in Figs.2.11, 4.3 and 4.4.

When a sample is located within the displacement range of the probe, the situation is different after the probe contacts the sample. Fig.4.5 shows the reflected wavelengths from S grating and M grating with a sample located at three different height positions, the first one at a high position, the second at middle position and the third at the low position. Each experiment was made as the probe went down from higher positions to lower positions and then contacted the silicon sample and indented into the sample. In the Fig.4.5, it is shown that the measurement follows the direction along the non-sample line
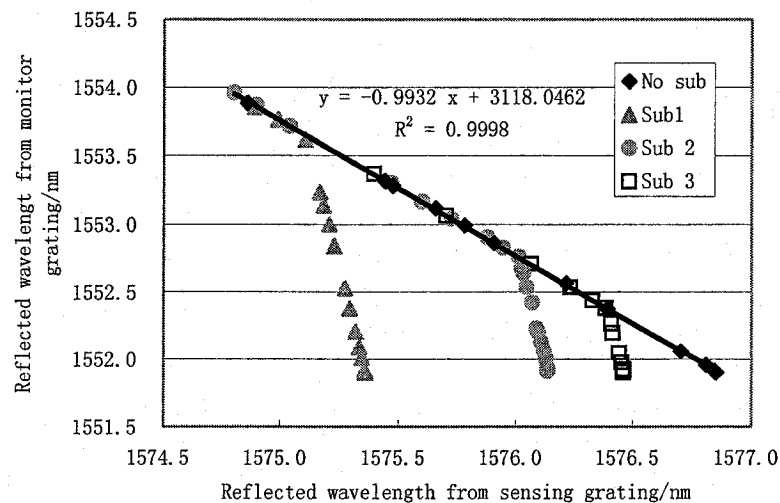
Fig. 4. 5. The reflected wavelengths from sensing and M grating fibers when a sample is located at three positions

(the solid line shown in Fig.4.5 or in Fig.4.4) from higher position to the lowers when no sample is met. When the load and probe meets the sample, the direction has to switch into

another way as shown as Sub 1, Sub 2 and Sub 3 in Fig.4.5. There were three curves out of the non-sample line, presenting three deformation processes at different heights. The three curves out of the solid straight line in Fig.4.5 are not the straight line parallel to the Y axis (the vertical axis) as the ideal sample theory described in Fig.2.13.b because in the real experiment, there is deformation existed between the probe and the sample. Thus, in the experiment, after the probe reaches the sample, the probe will still enter deeper and deeper into the sample when the probe continue to be forced, causing the displacement sensing grating fiber still elongate and the reflected wavelength still shift.

4.2.2 Variation of Force versus Deformation

An important significance of the measurement using two gratings is that it is capable of measuring the deformation between two materials while applying force. It is a simple method keeping the ability to sense probe's penetration depth, to sense the applied force and furthermore to control them, which has the potential to investigate both the plastic and elastic property of a material as well as an indentation measurement. Based on Fig.4.5, it can extract the relation between the force and the deformation by equations of (2.50) and (2.52). The result is shown in Fig. 4.6.

From Fig.4.6, it shows that as the applied force increases, the deformation increase. From the experiment, it is known that the deformation is sensitive to the applied force. To use the method to measure the step height, this deformation's influence have to be considered and controlled because the deformation value is in μm. By limited the force against the sample to control the deformation, the two-grating method can be used to measure the step height; by investigating the deformation under different applied forces, this method can additionally measure the hardness and modulus of the sample material as
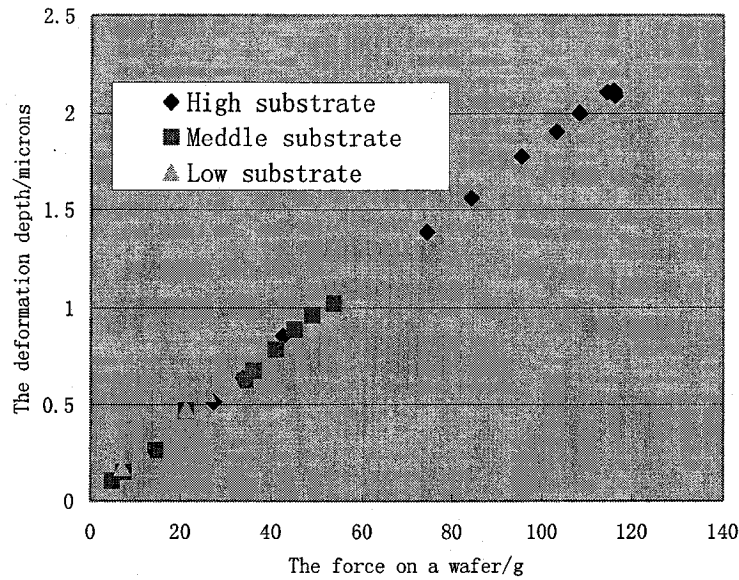
Fig. 4.6 Relation between the penetrated depth and the force against sample for three sample positions

described in following section.

4.2.3 Indentation Measurement Using Two FBGs

Two FBG measurement systems can be used as indentation measurement instrumentation because two gratings can sense displacement and the force against the sample separately. Two examples will show the indentation measurement application by
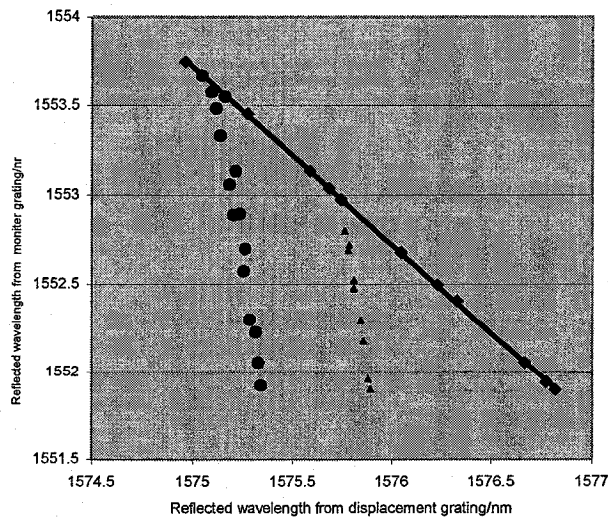
Fig. 4.7. Indentation measurement at two different region on a wafer at different height positions

using two FBGs.

In this experiment, we measured two different places of a silicon wafer located at two different heights within the displacement grating sensing range. Before doing the indentation measurement, the non-sample line is first measured without any sample within the range of the displacement sensing grating, then following the two indentation measurements. The measured results are presented in Fig.4.7. The detail results of indentation measurement at two positions are shown in Fig.4.8.a and b. One indentation measurement for one position measurement includes two processes. The first is called loading process and the second is called unloading process. In the loading process, after the probe has been lowered down to reach the surface of the sample, the load was increased to make the probe penetrate into the sample deeper and deeper. The maximum load can be applied to sample depends on the height of the sample within the range of the displacement sensing grating. The higher the position at which a sample is located, the larger force exerted on the sample. The position 1 is higher than the position 2, the maximum applied force to the sample at the position 1 is 114.4gf while at position 2 is equal to 73gf.

Using data presented in Figs.4.8. a and b, the applied force and the penetrate depth curves (load-depth curve) are shown in Fig.4.9.a and b at two different heights. The penetration depth is the response of the measured material to the applied force. The mechanical properties' information of the material can be obtained from load-depth curve. For example in Fig.4.9.a, silicon is a material as a results an applied force more than 100 g causes only about $2\mu m$ deformation at its surface. Since the loading curve and the unloading curve are very close to each other in Fig.4.9, it can conclude that silicon is a low plastic material. The reason for that is loading curve includes both plastic and elastic

89

properties, but the unloading curve mainly contains elastic property.
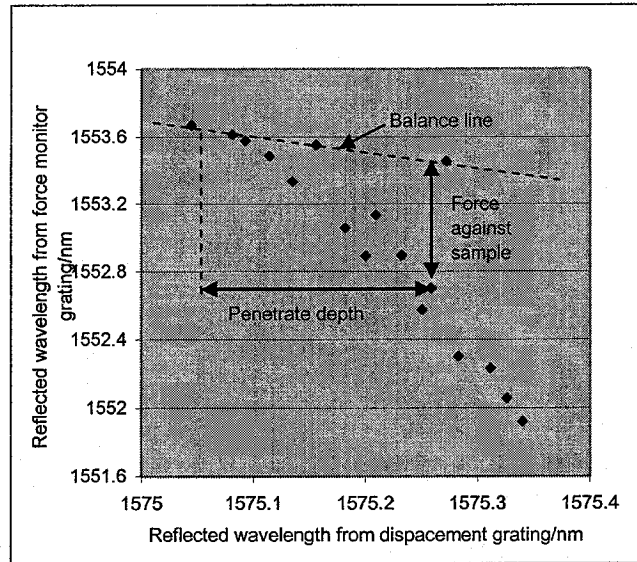
a
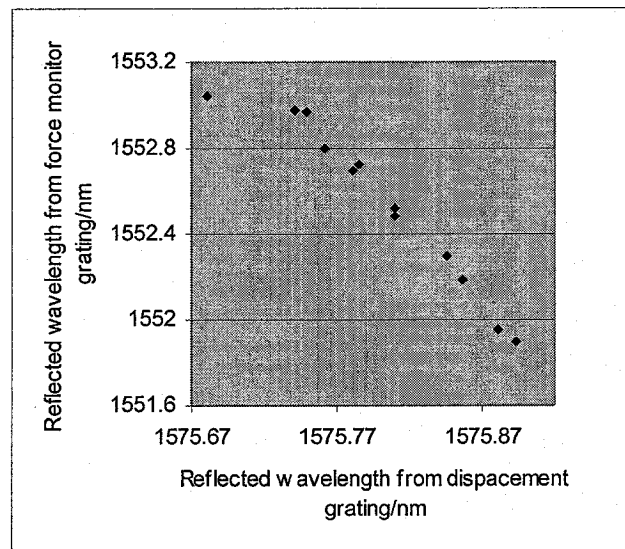
b

Fig. 4. 8. The detail measured data of indentation measurement at two positions.
a) at position 1. b) at position 2.
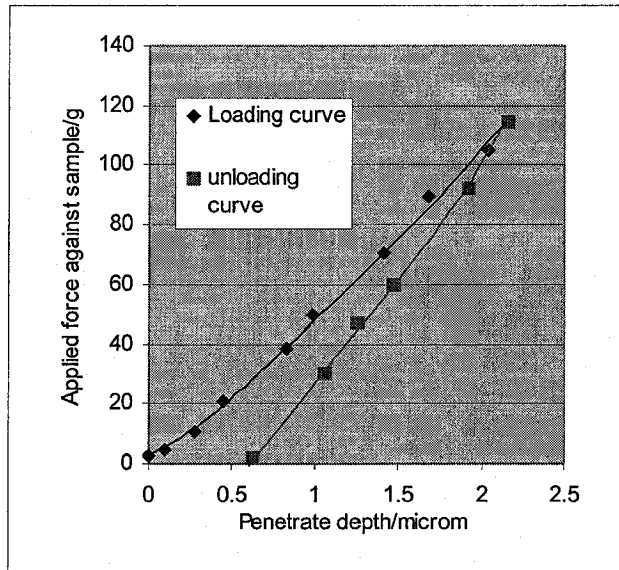
a
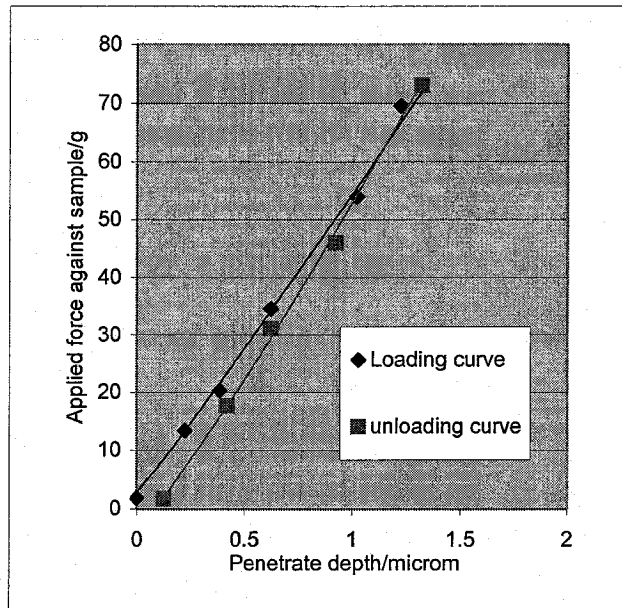
b

Fig. 4. 9. The detail measured data of indentation measurement at two positions.
a) at position 1. b) at position 2.

4.3 Step Height Measurement

The heights of etched steps were measured using the two-grating system.

The measurement was done point by point along a dash straight line in Fig.4.10 from the top surface at A to the bottom surface at A' in the direction perpendicular to the step on the sample. To implement the movement from one position to another, actually a horizontal translation stage was used to drive the sample to move. Before measurement a
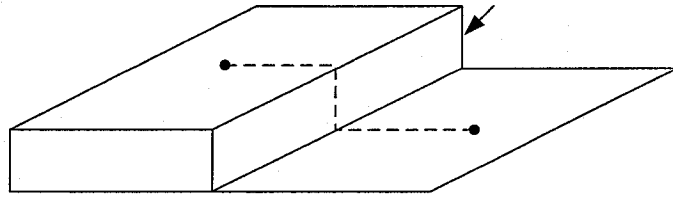
Fig. 4. 10 Step measurement

non-sample line was drawn without a sample within the measurement range. The probe was raised over the surface, and the sample was raised into the measurement range, then a point was chosen to measure. For every position for measurement as the probe was lowered down to approach the surface, touch the surface and make a little indentation into the surface, record the reflected wavelengths from the displacement sensing grating and the monitor grating. The surface height at a position was determined by the turning point that switches the non-sample line into the deformation curve in the graph of relation between reflected wavelengths from the S grating and the M grating. The step height was checked by SEM by the writer.

A step with 1.4 μm height was used to be measured by the two-grating system. There were 12 positions on the sample surface that were measured, 6 positions on the top surface and 6 positions on the bottom surface. The surface height at 12 positions with respect to reflected wavelengths from S grating was shown in Fig.4.11.a. The reflected

wavelength from M grating can be used for the step identification shown in Fig.4.11.b.

From Figs.4.11.a and 4.11.b, a step can be identified. The surface height at 12 positions

a   b
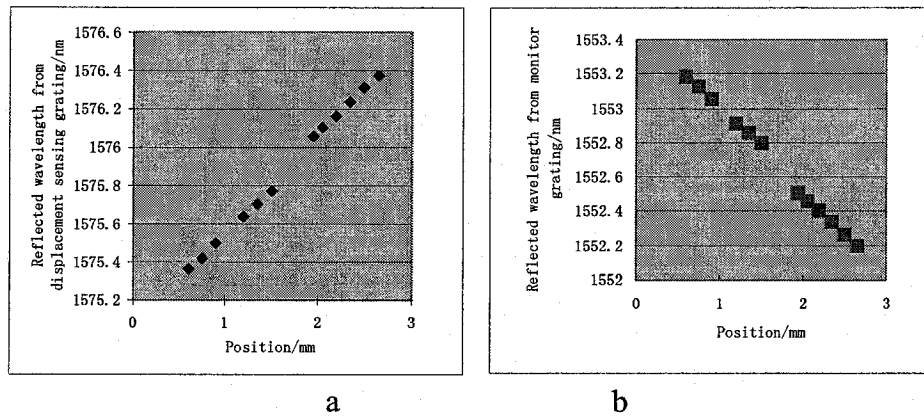
Fig. 4.11. Reflected wavelength from a) displacement sensing grating (D grating) and
b) force monitor grating (M) at different positions along a measured line
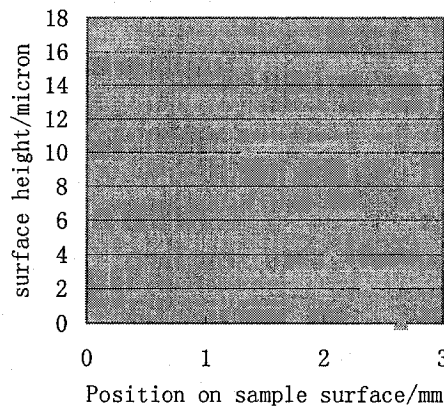
Fig. 4.12. The position height on the sample surface

were shown in Fig.4.12. From Fig4.12, it is clear that the surface of stage was tilted

although the surface was horizontally leveled prior to measurement. The tilted angle can be

calculated from Fig.4.12, and it was less than 0.3° (6 mrad). After the tilted angle was

cancelled by calculation, the surface heights at 12 positions were shown in Fig.4.13. From
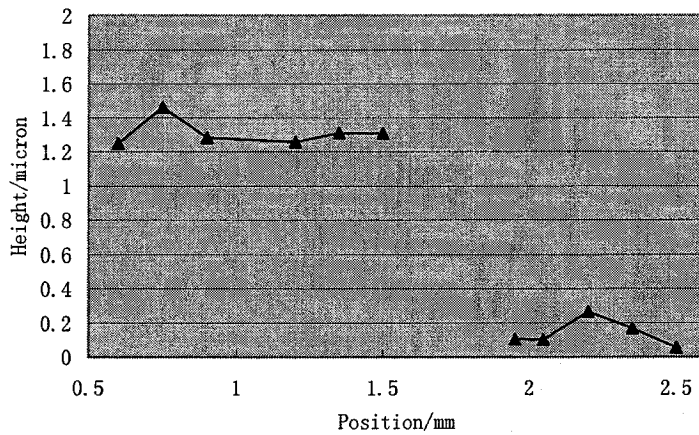
Fig4.13.Step height on a silicon sample

Fig.4.13, it is clear that the height of the step is about 1.2 μm. This step was checked by

SEM to be 1.4 μm.

4.4 Deformation Simulation Result

To understand the deformation between ruby probe and silicon wafer, the FEM was

used to analyze the deformation when ruby probe contact the wafer. The modeling, the

messing and other parameters used for the simulation were mentioned in Chapter III. Here,

the simulation result is presented.

The pressure on the top of the ruby changes from 0.100 MPa to 0. 860 MPa, which

corresponds to an equivalent change in the applied force on top of the ruby from 17gf to

143gf. Fig.4.14 shows the simulation result of the finite element analysis, where the

maximum displacement on top of the ruby is plotted with respect to the applied pressure.

For a particular case when the applied pressure is 0.5 Mpa (82gf), the 3D deformation

distribution of the half sphere probe and the silicon wafer is shown in Fig.4.15.

94
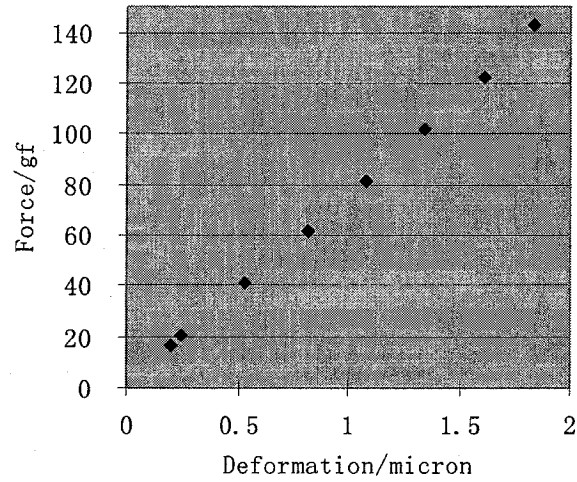
Fig. 4. 14. Maximum deformation versus the applied pressure
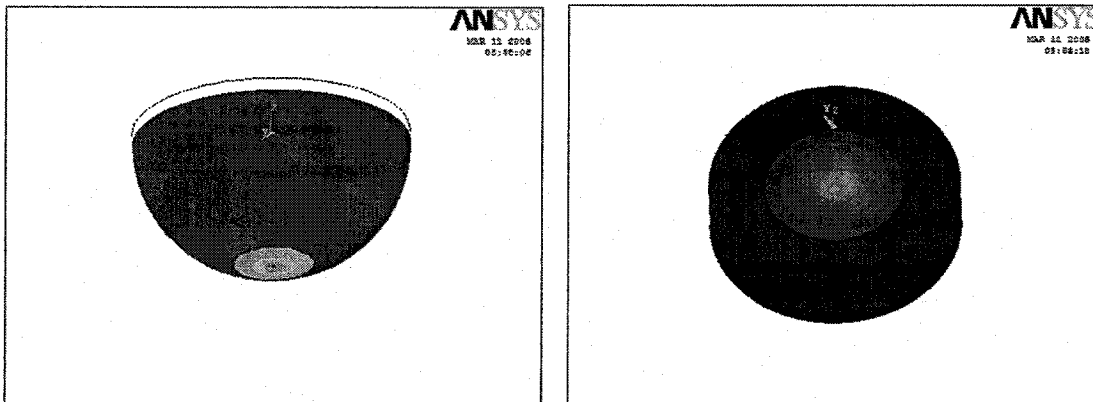
Fig. 4. 15. Deformation of the ruby and substrate under a 0. 5 MPa pressure

At first let us concern about maximum deformation points at ruby and silicon wafer, which are the bottom point of ruby and its contact point at silicon wafer. Fig.4.16 shows displacements of points along the Z axis (the symmetrical axis of two bodies) from the top of the ruby (DIST=0μm) to the bottom of the substrate (DIST=1220μm) when the pressure of 0.5 MPa or the force of 82gf is applied on the top surface of the ruby. From

95

Fig.4.16, we can see the moved distance of the point at top of the ruby is 0.91μm. The point

at bottom position of the ruby has moved 0.69 μm. Thus, the maximum deformation of

ruby is at its bottom point in value of 0.22μm(=0.91-0.69). There is no displacement of the

point at the bottom of the silicon wafer, and the maximum deformation point of the silicon

wafer is the one contacting with the bottom point of ruby, which has the deformation of

0.69μm.
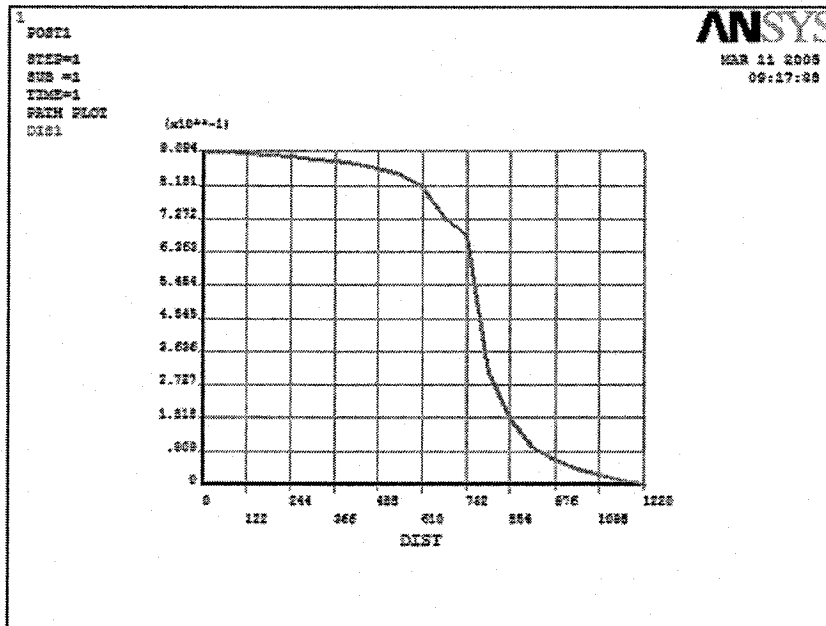
Fig. 4. 16. Movement distances of points along the structure from the top of the ruby (DIST=0)

to the bottom of the substrate (DIST=1220)

The simulation result is that when applied force of 82gf, the maximum

deformations of the ruby and the silicon wafer are 0.22μm and 0.69μm respectively. The

deformation of the ruby is less than that of silicon because the ruby is harder than the

silicon. The deformation of silicon is over 3 times more than that of ruby. The ruby probe

itself produced about 1/3 of total deformation indicates it is not good candidate as an

indenter for a silicon indentation measurement.

4.5 Discussion

In the one–grating indentation and two-grating indentation experiments, it can estimate that the total deformation is about 2.6 μm when applied 140gf load. These two methods can compare with each other.

The total deformation in FEM simulation in ANSYS is about 1.8 μm when applied about 140gf load. Although this simulation deformation value is less than the experimental result, it also compare with the experiment result because they are in the same order. One reason for the smaller simulation result may be the real tip of the probe in experiment is not in sphere shape and is smaller than that of simulation condition of 1.44mm diameter.

CHAPTER V

CONCLUSIONS AND SUGGESTIONS

This chapter summarizes the thesis, draws a conclusion, claims contributions and makes suggestions for future work.

5.1 Summary

Characterization of material surface properties requires varied measuring techniques. The characterization measurement using hard probe is a good way to detect the surface topography and the material mechanical properties. Controlling the applied force and sensing the displacement of the probe is the heart of this probe instrumentation. The fiber Bragg grating, a small portion in a periodic modulation of the refractive index in the core of an optical fiber, can play the role of sensing force and displacement. This thesis successfully introduced the Bragg grating for the first time in the characterization of material surface.

The fundamental principle of the displacement and the force sensing is the strain effect of FBG. A strain change of a FBG fiber can cause a shift of the reflected wavelength from the FBG fiber, which follows the law,

$$\Delta\lambda_B = \lambda_B \ (1-p_e)\varepsilon$$

Based on this formula and according to the strain definition and the Hooke's law, the displacement and the force sensing expressions can be derived as follows:

$$\Delta\lambda = \frac{\lambda_B(1-p_e)}{l_0}\Delta l$$

$$\Delta\lambda_B = \frac{\lambda_B(1-p_e)}{EA}F$$

where $\Delta\lambda_B$ is in nm. l and Δl is the length of the fiber and the fiber length change

respectively. These are two fundamental equations in the thesis.

Fine measurements using Bragg grating on a material surface are analyzed and the experiments are implemented. A Bragg grating can simply and linearly senses displacement and the force. These two sensing properties of the FBG were experimentally investigated by using long FBG fiber. Three long FBG fiber experiments provide the evidence of the feasibility of using FBG in the fine measurement system.

In the thesis, three instrumentation methods are proposed and experimentally implemented: one grating indentation measurement, two grating indentation measurement and step height measurement. The set-up of one grating indentation method is simple. The advantage of the two grating indentation and the step height methods is that use one grating to sense the displacement and use another to monitor and control the applied force against a sample.

In history, few investigations using FBG in displacement measurement were reported. Past research's interest on the displacement measurement is in the macro scale of ~mm. In this thesis FBG is applied in a fine displacement measurement. To my knowledge, no work using FBG appeared on the fine measurement in the scale of micro or less than $1\mu m$.

In this thesis, FBG used in sensing fine displacement and force is investigated. The displacement measurement sensitivity, the measurement range and the force against fiber and against sample is studied and used to design the experimental fine surface measurement system. A dual-grating displacement measurement method is proposed, which can double the sensitivity and is also temperature independent. The sensing length of FBG fiber and the characteristic reflected wavelength are two important factors to obtain

bigger value of the $\Delta\lambda_B$ and raise the measurement sensitivity and reliability. The force is analyzed and found that the force against fiber and force against sample depend on the probe's position within the measurement range.

Also a simple indentation measurement using one FBG is proposed. This indentation measurement may work in compressive and tensional ways. The proposed indentation measurement in tensional way is investigated. The load-depth curve, a typical curve of an indentation measurement, can be obtained from sample's upward and downward process. In one-grating system, including the dual grating system discussed in this chapter, a shift of reflected wavelength indicates both the displacement and the applied force.

A two–grating indentation measurement method is also proposed in this thesis. In the system, one FBG fibers is used to sense the fine displacement; another is the monitor grating fiber that is used to monitor and control not only the movement of the object of load and probe but also the load weight on sample and sample surface deformation (or probe penetration depth). The monitor grating fiber together with the displacement sensing grating fiber can separately sense the force against the sample and the displacement, capable to measure surface topography and mechanical properties.

In the two–grating indentation measurement, the relation between the reflected wavelength of the displacement sensing grating and that of the monitor grating without a sample and with a sample were investigated. The expressions of force against sample and the deformation between sample and probe were derived.

A high quality of OSA and other optical equipments were used to lead the experiments to good results. A ruby probe was manually made. A load was matel-worked

in Machine Shop. A leveler was manually made successfully. SEM was used to check step height of silicon samples etched by TMAH solution. Stage displacement is calibrated by displacement gauge. The indentation deformation of silicon made by the ruby probe was simulated in the environment of ANSYS.

5.2 Conclusion

The purpose of this thesis was to establish a new methodology to characterize material surface using the Bragg grating fiber technology.

FBG sensors can be regarded as a promising candidate to be applied to surface measurement instrumentation due to its dual sensing abilities for force and for displacement, small sensing part in size, simple uniaxial measurement configuration, linear responsive behavior and simple measurand interpretation.

This thesis has theoretically proposed and experimentally proved that FBG has the capability to be used not only in surface topography measurement but also in the indentation measurement to investigate the dynamical mechanical properties of the sample material.

One-grating system can be used in the indentation measurement. Two grating system can be used in the indentation measurement and the step height measurement.

5.3 Contributions

- Establish a new methodology in the material surface measurement using FBG;

- Introduce FBG into fine displacement detection;

- Use the two properties of sensing displacement and force together in one device;

- Theoretically analyzed and experimentally implemented an one-grating

indentation method;

- Theoretically analyzed and experimentally proved that a two-grating system can use one grating to sense displacement and another to sense force and furthermore can sense the applied force against sample and the deformation between the probe and the sample's surface;

- Theoretically analyzed and experimentally implemented two-grating indentation method and the step height measurement method;

- Propose a dual grating array system to enhance the displacement measurement sensitivity.

5.4 Suggestion

Suggestions are proposed as follows:

- The displacement and force measurement sensitivity need to improve if the surface measurement is used in the nano scale. This can be improved by etching the FBG fiber and changing the FBG fabrication process and the material of the fiber. Meanwhile, one can use the short length grating to improve the displacement sensitivity. As reported by Wu[55], the length of the grating can be as small as a few hundred microns.

- One grating indentation measurement system in compressive mode, which is described in 2.1.9 section of Chapter II, would be investigated. An advantage of this indentation system is its simplicity and only needs a fine diamond indenter connected to one end of FBG section. Furthermore, the length of the FBG section can be tailor-made by device maker.

- Choose diamond as a probe. The best choice for a probe is to use diamond. The

102

probe-wafer contact simulation result shows the ruby probe has about 1/3 of total

deformation, which is not good as an indenter for an indentation measurement for

the material like silicon.

REFERENCES

[1] Peng Gao and Zhejun Yuan, DESIGN NOTE, "Development of a micromechanical probe-measuring instrument for surface properties characterization", *Meas. Sci. Technol.* **10** N105–N108, 1999.

[2] Beck U, Smith D T, Reiners G and Dapkunas S J, "Mechanical properties of $SiO2$ and $Si3N4$ coatings: a BAM/NIST co-operative project," *Thin Solid Films* 332, 164–171, 1998.

[3] E.G. Herbert, G.M. Pharr , W.C. Oliver , B.N. Lucas , J.L. Hay, "On the measurement of stress–strain curves by spherical indentation", *Thin Solid Films* 398 –399 331–335, 2001.

[4] W. C. Oliver and G. M. Pharr, "An improved technique for determining hardness and elastic modulus using load and displacement sensing indentation experiments", *J. Mater. Res*. Vol. 7, No. 6, p. 1564,1992.

[5] B Wolf and A Richter, "The concept of differential hardness in depth sensing indentation", *New Journal of Physics,* 5 15.1–15.17, 2003.

[6] Mark R.VanLandingham, "Review of Instrumented Indentation" Journal of Research of the National Institute of Standards and Technology Vol. 108, Number 4, 249-265, 2003.

[7] Yang F Q "Effect of adsorption on nanoindentation test", *Appl. Phys. Lett.* Vol 80, Issue 6, 959–61,2002.

[8] Kasap, "Optoelectronics and Photonics Principles and Practices," Prentice Hall, p50, 2001.

[9] K.T.V Grattan, B.T. Meggitt, *Optical Fiber Sensor Technology: Fundamentals,* Kluwer Academic Publishers, 2000.

[10] Gerd Keiser, "Optical Fiber Communications," 3rd ed.,McGraw-Hill Book Company, 6-12,2001.

[11] Hill K. O, "Photosensitivity in optical fiber waveguides application to reflection filter fabrication" (J). *App. Phys. Lett.*, 32(10): 647-653,1978

[12] Zhi Zhou , Thomas W. Graver, Luke Hsu, Jin-ping Ou, "Techniques of Advanced FBG sensors: fabrication, demodulation, encapsulation and their application in the structural health monitoring of bridges," *Pacific Science Review*, vol. 5, pp.116~121, 2003.

[13] G. Meltz, W.W. Morey, W.H. Glenn, "Formation of Bragg Gratings in Optical Fibers by A Transverse Holographic Methos", *Optics Letters*, 14, 823 – 825, 1989

[14] Chi-Young Ryu and Chang-Sun Hong "TECHNICAL NOTE Development of fiber Bragg grating sensor system using wavelength-swept fiber laser", *Smart Mater. Struct.* 11 468–473, 2002.

[15] S. C. Tjin, Member, IEEE, R. Suresh, and N. Q. Ngo,"Fiber Bragg Grating Based Shear-Force Sensor:Modeling and Testing", *Journal of Lightwave Technology*, Vol. 22, No. 7, 1728-33, JULY 2004

[16] Mohanraj Prabhugoud and Kara Peters, "Modified Transfer Matrix Formulation for Bragg Grating Strain Sensors", *Journal of Lightwave Technology*, Vol.22, NO. 10, 2302, Oct 2004

[17] Sheng, H.-J., Ming-Yue Fu, Tzu-Chiang Chen, Wen-Fung Liu, Sheau-Shong Bo, "A lateral pressure sensor using a fiber Bragg grating" *Photonics Technology Letters*, IEEE, Volume: 16 , Issue: 4 , pp:1146 – 1148 April 2004.

[18] Bai-Ou Guan, Hwa-Yaw Tam, Shun-Yee Liu, "Temperature-independent fiber Bragg grating tilt sensor", *Photonics Technology Letters*, IEEE, Vol. 16, Issue: 1, 224 – 226, Jan.

2004

[19] Chen X., Zhou K., Zhang L., Bennion I., "Optical Chemsensor Based on Etched Tilted Bragg Grating Structures in Multimode Fiber", IEEE *Photonics Technology Letters*, Volume: PP , Issue: 99 , Pages:1 – 3, 2005.

[20] Hill K.O. "Bragg grating fabricated in monomode photosensitive optical fiber by UV exposure through a phase mask". *Appl. Phys. Letter*, 62(10):1035-1037,1993.

[21] Byoungho Lee, "Review of the present status of optical fiber sensors," *Optical Fiber Technology* 9 57–79, (2003).

[22] Yu Fan, Supervisor: Dr. Mojtaba Kahrizi "Characterization of Fiber Bragg Grating Sensor Array Embedded in Composite Structures" Master Thesis, ECE, Concordia University,Montreal, Quebec, Canada. Jan, 2004.

[23] Hideaki Iwaki, Hiroshi Yamakawa, and Akira Mita "FBG-Based displacement and strain sensors for health monitoring of smart strutures", Fifth International Conference on Motion and Vibration Control (MOVIC 2000), 4-8, Sydney, Australia, Dec. 2000.

[24] Yong Zhao, Chengbo Yu and Yanbiao Liao," Differential FBG sensor for temperature-compensated high-pressure (or displacement) measurement" *Optics & Laser Technology*; Vol. 36 Issue 1, p39, 4p,39-42: Feb 2004.

[25] Wenghong Yu, Hwayaw Tam, Zhiguo Liu, Wenghong Chung and Shuwei Geng, "Passive temperature compensation technique for fibre Bragg grating displacement sensor", *Electronics Letters* 9th. Vol.35, No.25, p2224-2226, December 1999.

[26] Weigang Zhang, Xiaoyi Dong, Qida Zhao, Guiyun Kai, and Shuzhong Yuan "FBG-Type Sensor for Simultaneous Measurement of Force (or Displacement) and Temperature Based on Bilateral Cantilever Beam" *IEEE Photonics Techotonics Letters,*

Vol. 13, No. 12, December 2001.

[27] Hay J L and Pharr G M, Instrumented indentation testing, *ASM Metals Handbook* (Materials Park, OH: ASM International) 2000.

[28] N. A. Burnham, R. J. Colton "Measuring the nanomechanical properties and surface forces of materials using an atomic force microscope" J *Vac. Sci. Technol.* A 7 2906, 1989.

[29] F Halitimy, N Ikhlefz, L Boudoukhax and G Fantozzix, "Microhardness, Young's modulus and fracture toughness of alumina implanted with Zr+, Cr+, Ti+ and Ni+. The effect of the residual stresses," *J.Phys. D: Appl. Phys.* 30 330–337,1997.

[30] Zinkle S J and Oliver W C "Mechanical Property Measurements on Ion-Irradiated Copper and Cu-Zr", *J. Nucl. Mater.* 141–143 548–552, 1986.

[31] McHargue C J, Sklad P S, McCallum J C and White C W "The structure of ion implanted ceramics" *Nucl. Instrum. Methods* B Vol 46, Issues 1-4, 74-78, 1 Feb 1990.

[32] Newey H M, Pollock and Wilkins M A, *Ion Implantation into Metals* ed V Ashworth (New York: Pergamon), 1982.

[33] Doerner M F and Nix W D, "A method for interpreting the data from depth-sensing indentation instruments", *J. Mater. Res.* 1(4) 601–9, 1986.

[34] Xiaodong Li, Liming Zhang and Hongsheng Gao, "Micro /nanomechanical characterization of a single decagonal AlCoNi quasicrystal", *J. Phys. D: Appl. Phys.* 37 753–757, 2004.

[35] Lawn D, *Fracture of Brittle Solid,* 2nd edn, Cambridge: Cambridge University Press, 1996.

[36] Lawn B R and Fuller E R, "Measurement of Thin-Layer Surface. Stresses by Indentation Fracture," *J. Mater. Sci.* 19 4061–7, 1984.

[37] O'Hern M E, McHargue C J, White C W and Farlow G C "The effect of chromium implantation on the hardness, elastic modulus, and residual stress of Al/sub 2/O/sub 3/" *Nucl. Instrum. Methods,* B **46** 171–5 1990.

[38] Fuqian Yang and Peixing Fei, "Microindentation of ground silicon wafers", *Semicond. Sci. Technol.* 19 1165–1168 PII: S0268-1242(04)76274-4, 2004.

[39] Wolf B, Bambauer K-O and Paufler P, "On the temperature dependence of the hardness of quasicrystals", *Mater. Sci. Eng.* A **298** 284, 2001.

[40] Richard C Appleyard, Michael V Swain, Sam Khanna3 and George A C Murrell "The accuracy and reliability of a novel handheld dynamic indentation probe for analysing articular cartilage", *Phys. Med. Biol.* **46** 541–550, 2001.

[41] Paufler P and Wolf B Deformation of quasicrystals by indentation *Quasicrystals: Structure and Physical Properties* ed Hans-Rainer Trebin (Weinheim: Wiley-VCH GmbH & Co. KGaA) p 501, 2003.

[42] Rami K Korhonen Simo Saarakkala, Juha Toyras1, Mikko S Laasanen, Ilkka Kiviranta and Jukka S Jurvelin, "Experimental and numerical validation for the novel configuration of an arthroscopic indentation instrument", *Phys. Med. Biol.* **48** 1565–1576 PII: S0031-9155(03)57658-8,2003.

[43] Dub S, Novikov N and Milman Y, "The transition from elastic to plastic behaviour in an Al-Cu-Fe quasicrystal studied by cyclic nanoindentation", *Phil. Mag.* A **82** 2161, 2002.

[44] ISO/FDIS 14577-1:2002; *Metallic materials - Instrumented indentation test for hardness and materials parameters,* ISO Central Secretariat,Rue de Varembé 1, 1211 Geneva, Switzerland, 2002.

[45]B J Briscoet, K S Sebastian and M J Adamst, "The effect of indenter geometry on the

elastic response to indentation," *J. Phys. D Appl.* Phys. 27 1156-1162,1994.

[46] P Berthoud, C G'Sell and J-M Hiver, "Elastic–plastic indentation creep of glassy poly(methyl methacrylate) and polystyrene: characterization using uniaxial compression and indentation tests", *J. Phys. D: Appl. Phys.* 32, 2923–2932, 1999.

[47] A. Otghonos, K. Kalli, *Fiber Bragg Gratings, Fundamentals and Applications in Telecommunications and Sensing*, Artech House, 1999.

[48] Kenneth O. Hill and Gerald Meltz, Member, IEEE, "Fiber Bragg Grating Technology Fundamentals and Overview"(*Invited Paper*), *Journal of Lightwave Technology*, Vol. 15, NO. 8, AUGUST 1263-1276, 1997.

[49] Yun-Jiang Rao, "In-fibre Bragg grating sensors" (Review Article),*Meas. Sci. Technol.* 8 355–375,1997.

[50] S.M. Melle, K. Liu, R.M. Measures, "Practical Fiber-Optic Bragg Grating Strain Gauge System", *Applied Optics*, Vol. 32, No. 19, 3601 – 3609, July 1993.

[51] G. Mahlke, P. Gössing, " Optical Fiber Cables, Fundamentals Cable Engineering Systems Planning", Siemens Aktiengesellschaft, 1993.

[52] "The Importance of Fiber Geometry", Corning Fiber News & Views, Dec. 1999.

[53] K Sadeghipourt, W Chent and G Barant "Spherical m icro-i ndentation process of polymer-based materials: a finite I element study", *J. Phys. D Appl. Phys.* 27 130M310,1994.

[54] O.Tabata, "Anisotropic etching of silicon in TMAH solution", *Sensors and Materials*, Vol.13, No.5, p271-283, 2001.

[55] Meng-Chou Wu, Robert S. Rogowski, "Fabrication of Self-Apodized Short-Length Fiber Bragg Gratings", *Applied Optics*, Vol. 42, Issue 25, 5017-5023, September 2003.